

On the Origin of Exponential Galaxy Disks

Aaron A. Dutton^{1*}

¹*UCO/Lick Observatory, University of California, Santa Cruz, CA 95064*

submitted to MNRAS

ABSTRACT

One of the most important unresolved issues for galaxy formation theory is to understand the origin of exponential galaxy disks. We use a disk galaxy evolution model to investigate whether galaxies with exponential surface brightness profiles can be produced in a cosmologically motivated framework for disk galaxy formation. Our model follows the accretion, cooling, and ejection of baryonic mass, as a function of radius, inside growing dark matter haloes. The surface density profile of the disk is determined by detailed angular momentum conservation, starting from the distribution of specific angular momentum as found in cosmological simulations. Exponential and quasi-exponential disks can be produced by our model through a combination of supernova driven galactic outflows (which preferentially remove low angular momentum material), intrinsic variation in the angular momentum distribution of the halo gas, and the inefficiency of star formation at large radii. We use observations from the SDSS NYU-VAGC to show that the median Sérsic index of late-type galaxies is a strong function of stellar mass. For blue galaxies, low mass galaxies have $n \simeq 1.3$, while high mass galaxies have $n \simeq 4$, with a transition mass of $M_{\text{star}} \simeq 2.5 \times 10^{10} M_{\odot}$. Our model with energy driven outflows correctly reproduces this trend, whereas our models with momentum driven outflows and no outflows over predict the Sérsic indices in low mass galaxies. We show that the observed fraction of “bulge-less” exponential galaxies is a strong function of stellar mass. For Milky-Way mass galaxies ($V_{\text{rot}} \simeq 220 \text{ km s}^{-1}$, $M_{\text{star}} \simeq 10^{11} M_{\odot}$) less than 0.1% of blue galaxies are bulge-less, whereas for M33 mass galaxies ($V_{\text{rot}} \simeq 120 \text{ km s}^{-1}$, $M_{\text{star}} \simeq 10^{10} M_{\odot}$) bulge-less and quasi-bulge-less galaxies are more common, with 45% of blue galaxies having Sérsic index $n < 1.5$. These results suggest that the difficulty of hierarchical formation models to produce bulge-less Milky-Way mass galaxies is, in fact, not a problem. However, the problem of producing M33 like galaxies remains, and will provide a key test for hierarchical galaxy formation models, and feedback models in particular.

Key words: galaxies: formation – galaxies: fundamental parameters – galaxies: haloes – galaxies: kinematics and dynamics – galaxies: spiral – galaxies: structure

1 INTRODUCTION

In the current paradigm for galaxy formation, set forth by White & Rees (1978) and Fall & Efstathiou (1980), disk galaxies are considered to form through the cooling of baryons inside dark matter haloes that grow by means of gravitational instability and acquire angular momentum from cosmological torques. In this paradigm the baryons acquire the same distribution of specific angular momentum as the dark matter, and this is conserved during cooling. Analytic models based on these assumptions have been able to produce disk sizes that are in reasonable agreement with observations (e.g. Dalcanton, Spergel & Summers 1997;

Mo, Mao & White 1998; de Jong & Lacey 2000; Dutton et al. 2007). In this picture the large scatter in disk sizes (including the existence of low surface brightness galaxies) is a natural consequence of the large scatter in halo spin parameter.

However, detailed hydro-dynamical simulations aimed at investigating the process of galaxy formation have indicated a potentially important problem for the cold dark matter (CDM) model. In CDM cosmologies, haloes form hierarchically by the merging of many lower mass haloes. Because the cooling in dense, low-mass haloes is very efficient, the baryons in these systems have already cooled by the time they merge with the more massive protogalaxy. They reach the center of the potential well by means of dynamical friction, through which they lose a significant fraction of their

* dutton@ucolick.org

angular momentum to the dark matter. Consequently, the disks that form in these simulations are an order of magnitude too small (Navarro & Benz 1991; Navarro & White 1994; Navarro & Steinmetz 2000). This is known as angular momentum catastrophe.

Attempted solutions to this problem include stellar feedback and/or ionizing background radiation which can prevent the cooling of the gas in low-mass haloes, thereby reducing the angular momentum loss (e.g. Domínguez-Tenreiro, Tissera & Sáiz 1998; Weil, Eke & Efstathiou 1998; Sommer-Larsen, Gelato & Vedel 1999; Eke, Efstathiou & Wright 2000; Maller & Dekel 2002). An alternative suggestion has been to reduce the number of low mass haloes by reducing the amplitude of the power spectrum on small scales (e.g. Kamionkowski & Liddle 2000; Sommer-Larsen & Dolgov 2001). However, these effects have only partially successful in resolving the angular momentum catastrophe. More recent numerical simulations have shown that in addition to feedback, very high numerical resolution is also required in order to avoid numerical angular momentum losses (e.g. Kaufmann et al. 2007; Ceverino & Klypin 2007; Mayer et al. 2008).

A second problem, related to angular momentum, is to understand the exponential density profile of stellar galactic disks. If disk galaxies form as envisaged in the standard picture their resulting surface density distribution is directly related to the specific angular momentum distribution of the protogalaxy. Motivated by the work of Mestel (1963), Crampin & Hoyle (1964) and Gunn (1982), Dalcanton et al. (1997) made the assumption that the protogalaxy has the AMD of a uniform sphere in solid body rotation, and showed that the resulting disks are more concentrated than exponential.

Firmani & Avila-Reese (2000) and van den Bosch (2001) refined this model by following the build-up and evolution of the disk density profile within a (cosmologically motivated) growing dark matter halo. In these models each shell of collapsing material is assumed to have the angular momentum distribution of a shell in solid body rotation, and the normalization of the angular momentum distribution is calculated by assuming that the spin parameter of the halo is independent of redshift. In the Firmani & Avila-Reese (2000) model the baryonic mass fraction of the galaxy was treated as a free parameter, with a fiducial value of 0.05. In the standard CDM cosmology (i.e. $\Omega_{m,0} = 1$), such a baryon fraction is consistent with the universal value. However, with the currently favored Λ CDM cosmology (where $\Omega_{m,0} \simeq 0.26$) the baryon fraction is $\simeq 0.17$, and the low baryons fractions in observed galaxies require an explanation. In the van den Bosch (2001) model the galaxy mass fraction is determined by the efficiencies of cooling and supernova (SN) driven outflows. Cooling is very efficient in galaxy mass halos, thus in order to produce the low galaxy mass fractions that are observed (e.g. Hoekstra et al. 2005; Mandelbaum et al. 2006) and required to reconcile the stellar and halo mass functions (e.g. Yang et al. 2007; Conroy & Wechsler 2008) galactic outflows are needed.

The van den Bosch (2001) model highlights the problem of producing pure exponential stellar galactic disks in a cosmological framework. In these models the disk may be approximately exponential over a few scale lengths, but the disk is invariably more concentrated than exponential

in the center. A potential short-coming of the Firmani & Avila-Reese (2000) and van den Bosch (2001) models is the assumption that the accreting mass shells have the AMDs of shells in solid body rotation.

Bullock et al. (2001b) determined the distribution of specific angular momentum in Λ CDM haloes from cosmological N-body simulations, and again concluded that these distributions will form overly concentrated disks. This excess of low angular momentum material has been confirmed by a number of subsequent studies (van den Bosch et al. 2002; Chen et al. 2003; Sharma & Steinmetz 2005). These simulations also indicated that CDM haloes have an excess of high specific angular momentum material, relative to that required to make an exponential disk. Furthermore, not even a single bulge-less disk galaxy with an exponential stellar density profile has been formed in hydrodynamical simulations in the Λ CDM paradigm. Thus one of the most important unresolved issues in galaxy formation is to understand the origin of the exponential profile of stellar galactic disks.

There are several reasons why the specific angular momentum profile of the stellar disk may be different than that of the dark matter and hot gas. Firstly only a fraction of the hot gas will be able to cool; secondly some of the cooled gas may be ejected from the galaxy or progenitor galaxies (e.g. Maller & Dekel 2002) via SN driven winds; thirdly only a fraction of the cooled gas will be converted into stars. Furthermore the surface brightness profile in optical light may not reliably trace the surface density profile in stellar mass. Thus an important question is whether the processes of star formation, feedback and stellar populations can produce exponential surface brightness profiles. If this is not possible then it signals that the cold baryons acquire a different distribution of specific angular momentum than the dark matter, or more fundamentally signals a failure of the CDM paradigm of structure formation.

In this paper we use the models described in Dutton & van den Bosch (2008), which are an updated version of the models used by van den Bosch (2001, 2002) to investigate the origin of the exponential light profiles of galactic disks. This model includes the detailed cooling, star formation and ejection of gas, as a function of radius, inside growing dark matter haloes with cosmologically motivated density profiles and angular momentum distributions.

This paper is organized as follows. In §2 we give an overview of the models, in §3 we discuss the impact of the initial angular momentum distribution, star formation, feedback, halo mass, adiabatic contraction and stellar populations on the structure of galaxy disks. In §4 we use observations from the SDSS to determine how frequent bulge-less galaxy disks are, and in §5 we make a comparison between these observations and Monte Carlo model samples. We discuss our results in §6 and give a summary in §7.

2 DISK GALAXY EVOLUTION MODELS

Here we give a brief overview of the disk galaxy evolution model used in this paper. This model is described in detail in Dutton & van den Bosch (2008; hereafter DB08). The key difference with almost all disk evolution models is that in this model the inflow (due to gas cooling), outflow (due to SN driven winds), star formation rates, and metallicity, are

computed as a function of radius, rather than being treated as global parameters. The main assumptions that characterize the framework of our models are the following:

(i) Dark matter haloes around disk galaxies grow by the smooth accretion of mass which we model with the Wechsler et al. (2002) mass accretion history (MAH). The shape of this MAH is specified by the concentration of the halo at redshift zero;

(ii) The structure of the halo is given by the NFW profile (Navarro, Frenk, & White 1997), which is specified by two parameters: the mass and concentration. The evolution of the concentration parameter is given by the Bullock et al. (2001a) model with parameters (Macciò et al. 2008) for a WMAP 5th year cosmology (Dunkley et al. 2009);

(iii) Gas that enters the halo is shock heated to the virial temperature, and acquires the same distribution of specific angular momentum as the dark matter. We use the angular momentum distributions of the halo as parametrized by Bullock et al. (2001b) and Sharma & Steinmetz (2005);

(iv) Gas cools radiatively, conserving its specific angular momentum, and forms a disk in centrifugal equilibrium;

(v) Star formation occurs according to a Schmidt (1959) type law on the dense molecular gas, which is computed following Blitz & Rosolowsky (2006);

(vi) SN feedback re-heats some of the cold gas, ejecting it from the disk and halo;

(vii) Stars eject metals into the inter stellar medium, enriching the cold gas.

(viii) Bruzual & Charlot (2003) stellar population synthesis models are convolved with the star formation histories and metallicities to derive surface brightness.

Each model galaxy consists of five mass components: dark matter, hot halo gas, disk mass in stars, disk mass in cold gas, and ejected gas. The dark matter and the hot gas are assumed to be distributed in spherical shells, the disk mass is assumed to be in infinitesimally thin annuli. Throughout this paper we refer to R as radius, t as time (where $t = 0$ is defined as the Big Bang) and z as redshift.

For each galaxy we set up a radial grid with 200 bins quadratically sampled from between 0.001 and 1 times the redshift zero virial radius. As described in DB08 for the purpose of conserving angular momentum it is more convenient to use a grid in specific angular momentum, j . We convert the initial grid in R , to a grid in j using $j^2/G = RM(R)$, where $M(R)$ is the halo mass enclosed within a sphere of radius R . We follow the formation and evolution of the galaxy using 400 redshift steps, quadratically sampled from $z = 10$ to $z = 0$. For each time step we compute the changes in the various mass components in each radial bin.

2.1 Angular Momentum Distribution

The radius at which the cooled gas ends up depends on its specific angular momentum, j . Van den Bosch (2001; 2002) assumed the j -distribution to be that of a shell in solid body rotation. In this paper we adopt cosmologically motivated specific angular momentum distributions (AMD).

The AMD can be specified by 2 parameters: a normalization (λ) and a shape (μ , or α). Both the normalization and shape parameters are log-normally distributed, with significant scatter. We assume that the spin and shape param-

eters are uncorrelated, although Bullock et al. (2001b) show that there may be a weak correlation between μ and λ , which needs to be investigated further.

The spin parameter is defined by

$$\lambda = \frac{J_{\text{vir}}|E_{\text{vir}}|^{1/2}}{GM_{\text{vir}}^{5/2}}, \quad (1)$$

where M_{vir} , J_{vir} , and E_{vir} are the mass, total angular momentum and energy of the halo, respectively.

Bullock et al. (2001b; hereafter B01) showed that dark matter haloes in a Λ CDM cosmology have specific angular momentum profiles that are well fitted by

$$m(j) = \frac{M(< j)}{M_{\text{vir}}} = \mu \frac{j/j_{\text{max}}}{j/j_{\text{max}} + \mu - 1}. \quad (2)$$

Here $M(< j)$ is the halo mass with specific angular momentum less than j , M_{vir} is the halo's virial mass, μ is a free parameter, and j_{max} is the maximum specific angular momentum in the halo. The value of j_{max} is given by

$$j_{\text{max}} = \frac{J_{\text{vir}}/M_{\text{vir}}}{(\mu - 1)[- \mu \ln(1 - \mu^{-1}) - 1]}, \quad (3)$$

where $J_{\text{vir}}/M_{\text{vir}}$ is determined by the spin parameter. B01 found $\mu - 1$ to be log-normally distributed with a mean and standard deviation in $\log(\mu - 1)$ of $\simeq -0.6$ and $\simeq 0.4$, respectively.

Sharma & Steinmetz (2005, hereafter SS05) used a series of non radiative N-body/SPH simulations in a Λ CDM cosmology to study the growth of angular momentum in galaxy systems. SS05 showed that Eq. 2 is unable to describe the specific angular momentum distribution required to make an exponential disk in an NFW halo. They introduced an alternative function that is able to describe the specific angular momentum distribution of exponential disks, as well as those of the gas and dark matter in their simulations.

$$m(j) = \gamma(\alpha, \frac{j}{j_d}), \quad j_d = \frac{J_{\text{vir}}}{M_{\text{vir}}} \frac{1}{\alpha} \quad (4)$$

where γ is the incomplete gamma function. SS05 found the distributions of α is log-normally distributed with mean $\log \alpha \simeq -0.05$, standard deviation in $\log \alpha \simeq 0.11$.

2.2 Conservation of Angular Momentum and Halo Contraction

In order to ensure that specific angular momentum is conserved in our model, rather than keeping track of how much mass is at a given radius, R , we keep track of how much mass is at a given specific angular momentum, j . Thus, under the simplifying assumption that $V_{\text{circ}} = [GM(< R)/R]^{1/2}$, where $M(< R)$ is the total mass within a spherical radius, R , the radius that corresponds to a given j is given by

$$R = \frac{j^2}{GM(< j)}. \quad (5)$$

This has a number of desirable properties: 1) At each time step it is trivial to calculate how much cold gas is added to each bin in j . 2) Over time, as the potential well changes, the specific angular momentum of the baryons is automatically conserved; 3) The adiabatic contraction (Blumenthal et al. 1986) of the halo in response to the cooling of the

baryons is automatically taken into account. 4) The resulting radial grid is adaptive, as the mapping between j and R depends on the amount of mass enclosed.

As discussed in Dutton et al. (2007) and DB08, models with halo contraction (and standard stellar IMF's) are unable to reproduce the zero points of the VMR relations as well as the low galaxy formation efficiency required to reconcile the halo mass function and galaxy stellar mass function. While there are processes such as dynamical friction and impulsive mass loss that can expand the halo, implementing these in a galaxy evolution model is a non-trivial task. Thus for simplicity we wish to consider a model in which the dark halo does not respond to galaxy formation. To calculate the mapping between j and radius, for the case of *no adiabatic contraction*, we solve the equation

$$R = \frac{j^2/G}{M_{\text{halo}}(R) + M_{\text{disk}}(< j)}, \quad (6)$$

where $M_{\text{halo}}(R)$ is the mass (within a spherical radius R) of the dark matter plus hot gas halo in the absence of galaxy formation, and $M_{\text{disk}}(< j)$ is the mass of the disk (gas plus stars) with specific angular momentum less than j . This way the self-gravity of the disk is included but adiabatic contraction is ignored.

2.3 Star Formation

Following Blitz & Rosolowski (2006) we assume that star formation takes place in dense molecular gas, traced by hydrogen cyanide (HCN), with a constant star formation efficiency:

$$\frac{\Sigma_{\text{SFR}}}{[M_{\odot}\text{pc}^{-2}\text{Gyr}^{-1}]} = \frac{\tilde{\epsilon}_{\text{SF}}}{[\text{Gyr}^{-1}]} \frac{\Sigma_{\text{mol,HCN}}}{[M_{\odot}\text{pc}^{-2}]}, \quad (7)$$

where $\tilde{\epsilon}_{\text{SF}} \simeq 10 - 13\text{Gyr}^{-1}$ (Gao & Solomon 2004, Wu et al. 2005). Expressing this equation in terms of the total gas content:

$$\frac{\Sigma_{\text{SFR}}}{[M_{\odot}\text{pc}^{-2}\text{Gyr}^{-1}]} = \frac{\tilde{\epsilon}_{\text{SF}}}{[\text{Gyr}^{-1}]} \frac{\Sigma_{\text{gas}}}{[M_{\odot}\text{pc}^{-2}]} f_{\text{mol}} \mathcal{R}_{\text{HCN}}, \quad (8)$$

where $\mathcal{R}_{\text{HCN}} = \Sigma_{\text{mol,HCN}}/\Sigma_{\text{mol}}$ is the ratio between the dense molecular gas (as traced by HCN) and the total molecular gas, and f_{mol} is the molecular gas fraction.

The fraction of gas that is molecular, f_{mol} , can be defined in terms of the mass ratio between molecular and atomic gas, \mathcal{R}_{mol} by

$$f_{\text{mol}} = \frac{\mathcal{R}_{\text{mol}}}{\mathcal{R}_{\text{mol}} + 1}. \quad (9)$$

Empirically Wong & Blitz (2002) and Blitz & Rosolowski (2004; 2006) have argued that \mathcal{R}_{mol} is determined to first order by the mid plane pressure, P_{ext} . The most recent relation from Blitz & Rosolowski (2006) is

$$\mathcal{R}_{\text{mol}} = \frac{\Sigma_{\text{mol}}}{\Sigma_{\text{atom}}} = \left[\frac{P_{\text{ext}}/k}{4.3 \pm 0.6 \times 10^4} \right]^{0.92 \pm 0.1}, \quad (10)$$

where k is Boltzmann's constant, and P_{ext}/k is in cgs units. For a gas plus stellar disk the mid plane pressure is given, to within 10% by (Elmegreen 1993)

$$P_{\text{ext}} \simeq \frac{\pi}{2} G \Sigma_{\text{gas}} \left[\Sigma_{\text{gas}} + \left(\frac{\sigma_{\text{gas}}}{\sigma_{\text{star}}} \right) \Sigma_{\text{star}} \right], \quad (11)$$

where σ_{gas} and σ_{star} are the velocity dispersions of the gas and stellar disk, respectively. For simplicity we will assume $\sigma_{\text{gas}}/\sigma_{\text{star}} = 0.1$.

Based on the arguments and references in Blitz & Rosolowski (2006) we adopt the following relation for \mathcal{R}_{HCN}

$$\mathcal{R}_{\text{HCN}} = 0.1 \left(1 + \frac{\Sigma_{\text{mol}}}{[200 M_{\odot}\text{pc}^{-2}]} \right)^{0.4}. \quad (12)$$

In the low pressure, low molecular density regime, $\mathcal{R}_{\text{HCN}} \simeq 0.1$, and thus Eq. (7) asymptotes to

$$\frac{\Sigma_{\text{SFR}}}{[M_{\odot}\text{pc}^{-2}\text{Gyr}^{-1}]} = \frac{\tilde{\epsilon}_{\text{SF}}}{[\text{Gyr}^{-1}]} \frac{0.013}{[M_{\odot}\text{pc}^{-2}]} \left(\frac{\Sigma_{\text{gas}}}{[M_{\odot}\text{pc}^{-2}]} \right)^{2.84}. \quad (13)$$

In the high pressure, high molecular density regime, $\mathcal{R}_{\text{HCN}} \propto \Sigma_{\text{mol}}^{0.4}$, and eq.(7) asymptotes to the familiar Schmidt-Kennicutt (SK) relation

$$\frac{\Sigma_{\text{SFR}}}{[M_{\odot}\text{pc}^{-2}\text{Gyr}^{-1}]} = \frac{\tilde{\epsilon}_{\text{SF}}}{[\text{Gyr}^{-1}]} \frac{0.012}{[M_{\odot}\text{pc}^{-2}]} \left(\frac{\Sigma_{\text{gas}}}{[M_{\odot}\text{pc}^{-2}]} \right)^{1.4}. \quad (14)$$

Furthermore, with $\tilde{\epsilon}_{\text{SF}} = 13\text{Gyr}^{-1}$, we recover the coefficient of $\epsilon_{\text{SF}} = 0.16$ of the standard SK relation.

We implement the star formation recipe given by Eq.(7) as follows. At each time step and annulus in the disk, we calculate the star formation rate. Then we use the following approximation (valid for times steps small compared to the star formation time scale) to calculate the mass of newly formed stars

$$\Delta M_{\text{star}}(R) = A(R) \Sigma_{\text{SFR}}(R, t) \Delta t, \quad (15)$$

with A the area of the annulus, and Δt the time step interval.

2.4 Supernova Feedback

We assume that SNe drive mass outflows, and that the outflows move at the local escape velocity of the disk-halo system. This choice is motivated by the fact that it maximizes the mass loss from the the disk-halo system (lower velocity winds will not escape the halo, and higher velocity winds will carry less mass).

For our energy driven wind model following Dekel & Silk (1986) we assume that the kinetic energy of the wind is equal to a fraction, ϵ_{EFB} , of the kinetic energy produced by SN. However, contrary to Dekel & Silk (1986) we apply this energy condition *locally* in the disk as a function of radius, rather than globally to the whole galaxy. Thus the mass ejected from radius, R , during a given time step is given by

$$\Delta M_{\text{eject}}(R) = \frac{2\epsilon_{\text{EFB}} E_{\text{SN}} \eta_{\text{SN}}}{V_{\text{esc}}^2(R)} \Delta M_{\text{star}}(R). \quad (16)$$

Here $\Delta M_{\text{star}}(R)$ is the mass in stars formed at radius, R , $E_{\text{SN}} = 10^{51}$ erg $\simeq 5.0 \times 10^7 \text{km}^2 \text{s}^{-2} M_{\odot}$ is the energy produced by one SN, and $\eta_{\text{SN}} = 8.3 \times 10^{-3}$ is the number of SN per solar mass of stars formed (for a Chabrier (2003) IMF).

Similarly for our momentum driven wind model we assume that the momentum of the wind is equal to a fraction, ϵ_{MFB} , of the momentum produced by SN, thus the mass ejected from radius, R , during a given time step is given by

$$\Delta M_{\text{eject}}(R) = \frac{\epsilon_{\text{MFB}} p_{\text{SN}} \eta_{\text{SN}}}{V_{\text{esc}}(R)} \Delta M_{\text{star}}(R). \quad (17)$$

Here $p_{\text{SN}} = 3 \times 10^4 M_{\odot} \text{km s}^{-1}$ is the momentum produced

by one SN, assuming that each SN produces $\simeq 10M_{\odot}$ of material moving at $v \simeq 3000 \text{ km s}^{-1}$ (Murray, Quataert & Thompson 2005). Note that this corresponds to a kinetic energy of $4.5 \times 10^7 M_{\odot} \text{ km}^2 \text{ s}^{-2} \simeq 10^{51} \text{ erg}$.

We assume that the ejected mass is lost forever from the system: the ejected mass is not considered for later infall, and the corresponding metals are not used to enrich the infalling gas. This is clearly a dramatic oversimplification, but we make this choice to maximize the amount of gas that is lost from the system.

2.5 Overview of Parameters

The input parameters of our models are as follows.

(1) Cosmology: $\Omega_{\text{m},0}, \Omega_{\Lambda}, \Omega_{\text{b}}, \sigma_8, h, n$. In this paper we adopt a flat Λ CDM cosmology motivated by the 5th year WMAP results (Dunkley et al. 2009), with $\Omega_{\text{m},0} = 0.258, \Omega_{\Lambda} = 0.742, \Omega_{\text{b}} = 0.044, \sigma_8 = 0.80, h = 0.7$, and $n = 1$.

(2) Halo structure: $K, F, \sigma_{\text{inc}}$. We adopt the Bullock et al. (2001a) model with $F = 0.01, K = 3.7$, and $\sigma_{\text{inc}} = 0.25$. These parameters reproduce the distribution of halo concentrations of relaxed dark matter haloes in cosmological N-body simulations (e.g. Wechsler et al. 2002; Macció et al. 2007; 2008)

(3) Angular momentum distribution: $\bar{\lambda}, \sigma_{\ln \lambda}, \alpha$ (or μ), $\sigma_{\log \alpha}$ (or $\sigma_{\log(\mu-1)}$). As fiducial values we adopt a median spin parameter $\bar{\lambda} = 0.025$ with a scatter $\sigma_{\ln \lambda} = 0.35$ (see DB08). For the angular momentum distribution we consider two fitting functions: the Bullock et al. (2001b) formula with median $\mu - 1 = 0.3, \sigma_{\log(\mu-1)} = 0.45$; and the Sharma & Steinmetz (2005) formula with a median $\alpha = 0.9$ and $\sigma_{\log \alpha} = 0.11$. For our fiducial model we adopt the Sharma & Steinmetz (2005) angular momentum profile.

(4) Star formation: $\tilde{\epsilon}_{\text{SF}}$. We use a star formation model based on dense molecular gas, which we compute following Blitz & Rosolowsky (2006). We adopt $\tilde{\epsilon}_{\text{SF}} = 13 \text{ Gyr}^{-1}$.

(5) Feedback: $\epsilon_{\text{EFB}}, \epsilon_{\text{MFB}}, \eta_{\text{SN}}, E_{\text{SN}}, p_{\text{SN}}$. We adopt an energy per SN of $E_{\text{SN}} = 10^{51} \text{ erg}$, a momentum per SN of $p_{\text{SN}} = 3 \times 10^4 M_{\odot} \text{ km s}^{-1}$, a SN rate of $\eta_{\text{SN}} = 4 \times 10^{-3}$ per solar mass of stars formed. We treat ϵ_{EFB} and ϵ_{MFB} as free parameters, with fiducial values of $\epsilon_{\text{EFB}} = 0.25, \epsilon_{\text{MFB}} = 0$.

(6) Stellar populations and chemical enrichment: $\mathcal{R}, y, Z_{\text{hot}}$, and the choice of initial mass function (IMF). We adopt the Chabrier IMF, a return fraction $\mathcal{R} = 0.35$, and a stellar yield $y = 0.02$, and a hot gas metallicity of 0.002 (i.e. $0.1Z_{\odot}$).

3 SURFACE DENSITY PROFILES

The surface density profile of a centrifugally supported disk is determined by two things:

- (i) the distribution of specific angular momentum (AMD), j , of the baryons (i.e. stars and cold gas); and
- (ii) the shape and amplitude of the rotation curve.

The AMD of the baryons may be modified from that produced by tidal torques, by inefficient cooling and SN driven outflows. The difference between the surface density profile of the stellar disk and baryonic disk is then determined by the (radially dependent) efficiency at which the cold

gas is turned into stars. Another complication is that observed light is a biased tracer of the stellar (and baryonic) mass. Below we discuss each of these effects for a fiducial model galaxy. This model has a total virial mass of $M_{\text{vir}} = 9.0 \times 10^{11} M_{\odot}$, a median halo concentration of this mass, and unless other-wise specified a halo spin parameter of $\lambda = 0.025$. This model also has no halo contraction, as models with halo contraction are unable to reproduce the zero points of the Tully-Fisher (TF) (Tully & Fisher 1977) and size-mass relations (DB08). However, as we show in §§3.5 & 5.4 none of our main results are sensitive to this assumption.

3.1 The Role of the Initial Angular Momentum Distribution

In the standard picture of disk galaxy formation the distribution of j of the cooled gas is the same as that of the hot gas and dark matter. As discussed in § 2, N-body simulations have shown that there is a universal j profile, described by one parameter (μ in B01; α in SS05). In Fig.1 we show the effect of the initial AMD shape parameter on the surface density and circular velocity profiles for our fiducial model galaxy. The upper panels use the B01 AMD with $\mu = 1.04, 1.11, 1.30, 1.90$, and 3.50 , while the lower panels use the SS05 AMD with $\alpha = 0.54, 0.69, 0.90, 1.15$, and 1.48 . For both AMD's these values correspond to the $-2, -1, 0, 1$, and 2σ of the distribution found in cosmological simulations.

In order to isolate the effects of the AMD from the effects of feedback, we fix the galaxy mass fraction and galaxy spin parameter to be equal to the values for a galaxy with $\alpha = 0.9$ and our favored energy driven feedback model ($\epsilon_{\text{EFB}} = 0.25$): $m_{\text{gal}} = 0.058$ and $\lambda_{\text{gal}} = \lambda = 0.028$.

Both the B01 and SS05 AMD's result in roughly the same surface density profiles and rotation curve shapes. The generic result is for lower values of μ and α to result in higher surface densities and circular velocities at small radii. As μ and α increase the central densities decrease and the circular velocity profiles become flatter. There are however two notable differences. The B01 profile has a maximum j , which results in a truncation in the surface density profile, this truncation occurs at a smaller radius for larger values of μ . The SS05 profile has less low angular momentum material for high values of α than the B01 angular momentum profile for high values of μ .

SS05 showed that the AMD at large j depends on the method used to calculate the AMD. In particular, the cell method used by B01 tends to result in a truncation of the AMD at large j , which is better fitted by the B01 profile. The particle method used by SS05 results in a smooth and extended AMD at large j , which is better fitted by the SS05 profile. If one removes the outer 5% of the j -distribution, SS05 showed that both profiles provide equally good fits to the AMDs computed using the cell and particle methods.

The concentration parameters for each model are given in Fig. 1. The concentration parameter of the stellar (C_{82s}) and baryonic disks (C_{82t}) are defined as the ratio between the radii enclosing 80 and 20% of the disk stellar/baryonic mass. For reference an exponential profile (Sérsic $n = 1$) corresponds to a concentration of $C_{82} = 3.6$, a Sérsic $n = 2$ profile corresponds to a $C_{82} = 5.8$, and a de Vaucouleurs profile (Sérsic $n = 4$) corresponds to a $C_{82} = 11.5$.

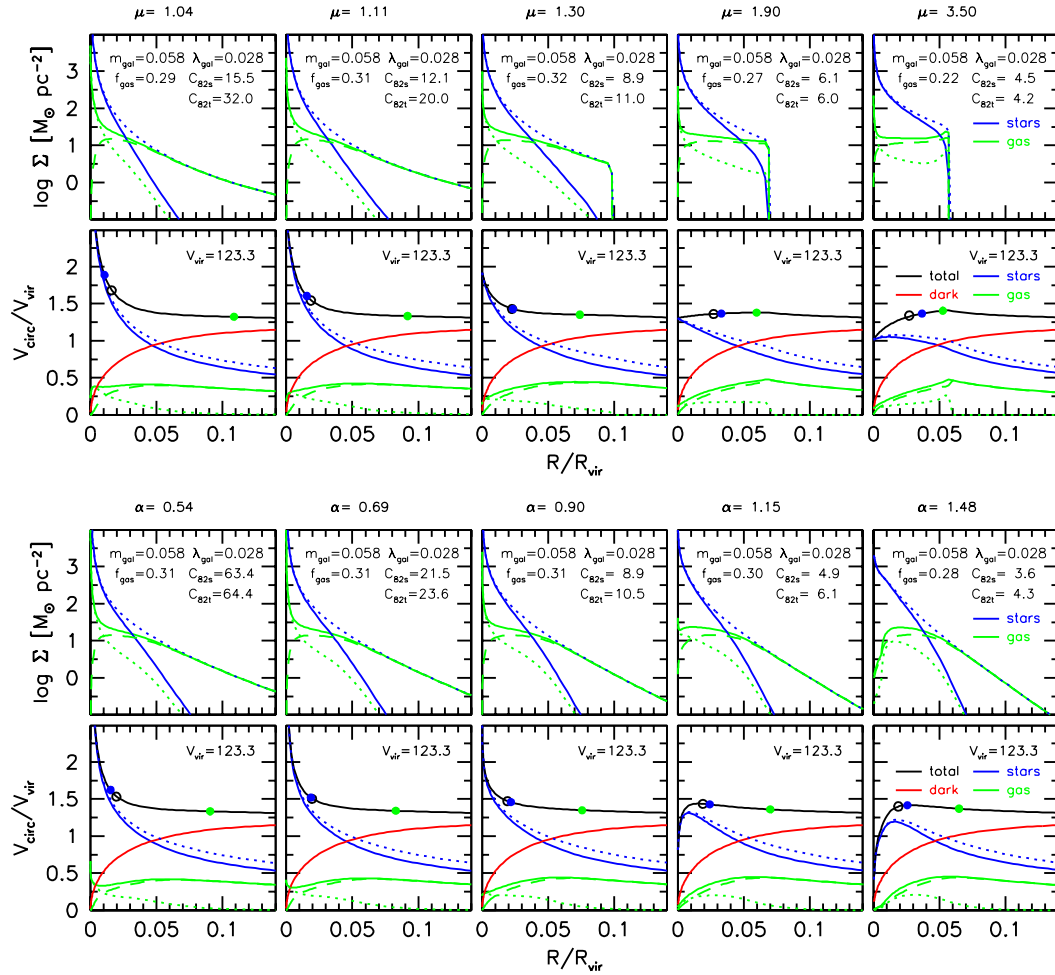


Figure 1. Effect of angular momentum shape parameter on surface density and circular velocity profiles. Radii are expressed in terms of the virial radius, R_{vir} , and velocities in terms of the circular velocity at the virial radius, V_{vir} . For the cosmology we adopt, the virial radius (in units of h_{70}^{-1} kpc) is $\simeq 2.068$ times the virial velocity (in units of km s^{-1}). All models have $m_{\text{gal}} = 0.058$, $\lambda = 0.028$, and $M_{\text{vir}} = 10^{11.8} h^{-1} M_{\odot}$. The upper panels use the B01 angular momentum profile (specified by μ), while the lower panels use the SS05 angular momentum profile (specified by α). The five values of the angular momentum shape parameter correspond to the mean, $\pm 1\sigma$ and $\pm 2\sigma$ of the distributions found in cosmological simulations. The stellar disk is given by the blue solid lines, the total disk by the blue dotted lines. The gas disk is given by the solid green lines, the molecular gas is given by the dotted green lines, and the atomic gas is given by the dashed green lines. The circular velocity of the halo is given by the solid red line and the total circular velocity is given by the solid black line. The circles show the circular velocity at three characteristic radii: 2.15 stellar disk scale lengths (black open circles); the radius enclosing 80% of the stellar mass, R_{80s} (blue filled circles); and the radius enclosing 80% of the cold gas mass, R_{80c} (green filled circles). For each model the cold gas fraction, f_{gas} , and stellar disk concentration, C_{82s} , and the baryonic disk concentration, C_{82t} , are given.

The B01 AMD results in less dispersion in the concentrations of the stellar and baryonic disks than the SS05 AMD, both at high and low values of α or μ . It should be noted that some of the very high concentrations $C_{82s} \simeq 100$ produced with the SS05 AMD are unrealistic. These are caused by the models having too much mass with low specific angular momentum, and our requirement that this specific angular momentum be conserved. In order for mass with low specific angular momentum to be in centrifugal equilibrium it has to be at small radii. However, when the baryons dominate the potential at small radii, this increases the circular velocity, which in turn requires the baryons move to even small radii, and so on. When centrifugal equilibrium

is reached, the inner disk is very compact. In practice the disk will become unstable before it reaches centrifugal equilibrium, and the baryons in the inner part of the galaxy will become at least partially supported by random motions, which will result in lower concentrations.

3.2 The Role of Star Formation

Fig. 1 also shows that the surface density profile of the stellar disk is very different than that of the total baryonic disk. The stellar disks are closer to exponential and have smaller sizes than the baryonic disks. These differences are due to the increased efficiency of star formation at higher gas den-

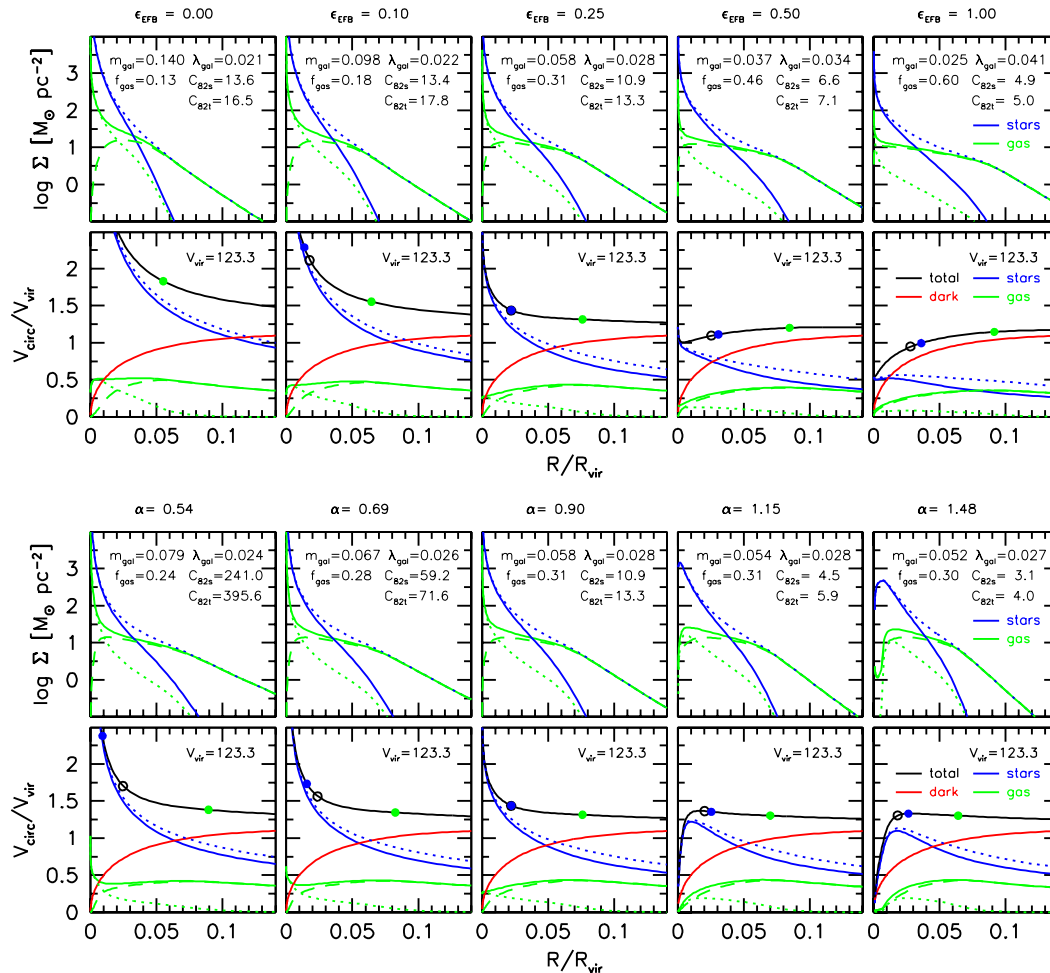


Figure 2. Effect of feedback on the surface density and rotation curves using the SS05 angular momentum profile. The upper panels have $\alpha = 0.9$ with ϵ_{EFB} varying from 0 to 1, while the lower panels have $\epsilon_{\text{EFB}} = 0.25$ with α varying over the 2σ range. The line types and colors are the same as in Fig.1. Without feedback (upper panels, far left) the model has too many baryons, which results in a disk that is too small, too concentrated, gas poor, and which rotates too fast. As the efficiency of feedback in increase (upper panels, from left to right), the baryon fraction decreases, which results in a larger disk, with lower concentration, higher gas fraction and lower rotation velocity. A model with maximal feedback (upper panels, far right) has a large, low concentration, gas rich disk, with a rising inner rotation curve.

sities (the Schmidt-Kennicutt law). More specifically, in the star formation model that we adopt, stars only form out of molecular gas, and the molecular fraction is a strong function of the surface density of stars and gas. In Fig. 1 the surface density of the molecular gas is given by the dotted green lines, and that for the atomic gas by green dashed lines. At small radii the gas is mostly molecular, whereas at large radii the gas is mostly atomic, and hence results in very inefficient star formation at low gas densities.

Our models thus predict that gas disks should have larger sizes than stellar disks, and that the baryonic disks are in general not exponential. Thus a study of the baryonic surface density profiles of galaxy disks would provide useful constraints to the initial AMDs and the efficiency of star formation at low gas densities.

An interesting consequence of the inefficiency of star formation at low gas densities, is that this results in a outer disk with a shorter scale length than the main disk. Such “disk breaks” are often seen in observed spiral galaxies (e.g.

Pohlen & Trujillo 2006). Why some galaxies show breaks, and others are purely exponential to large radii, and still others show anti-truncations (i.e. larger outer disk scale lengths), is an open question. If the efficiency of star formation at low gas densities varies between galaxies this could provide an explanation for the wide range in outer disk profiles observed in spiral galaxies. A study of baryonic disk density profiles would thus provide a means of distinguishing between a star formation efficiency origin vs a dynamical origin (e.g. Debattista et al. 2006; Younger et al. 2007; Roškar et al. 2008; Foyle, Courteau & Thacker 2008) for these features.

3.3 The Role of Feedback

The models in Fig. 1 had the galaxy mass fraction and spin parameter fixed. However, in a halo with $M_{\text{vir}} \simeq 9 \times 10^{11} M_{\odot}$, the cooling efficiency is high, such that in the absence of feedback the galaxy mass fraction is $\simeq 80\%$. In order to

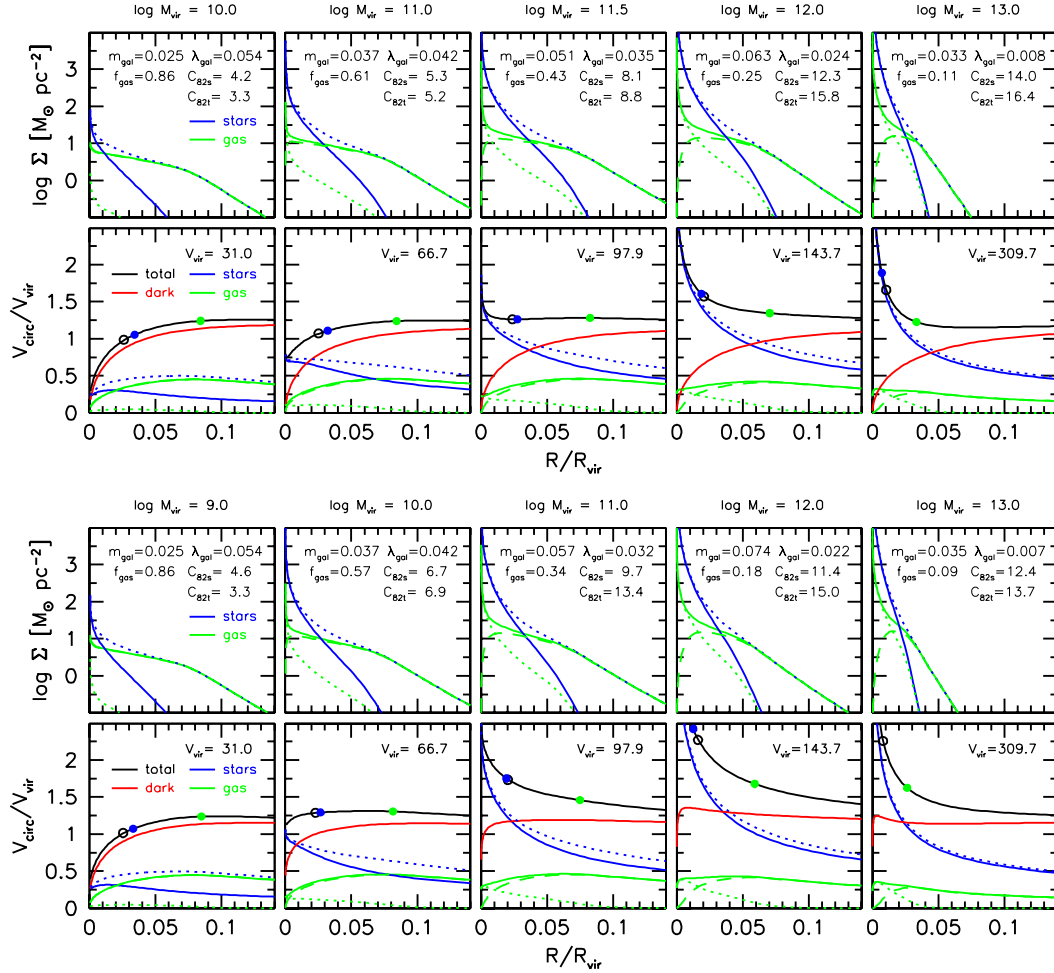


Figure 3. Effect of halo mass on surface density and circular velocity profiles in a model with feedback. All models have $\epsilon_{\text{EFB}} = 0.25$, $\alpha = 0.90$ and $\lambda = 0.025$. The redshift zero virial mass (in $h = 1$ units) is given above each column, the corresponding virial velocity is given in the velocity panels. The upper panels are for a model without adiabatic contraction, the lower panels include adiabatic contraction. The line types and colors are as in Fig. 1. Low mass haloes result in low galaxy mass fractions (m_{gal}), high galaxy spin parameters (λ_{gal}), high gas fractions (f_{gas}), low stellar concentrations ($C_{\text{S}2\text{s}}$), and dark matter dominated inner rotation curves. As halo mass increases m_{gal} increases (up until $M_{\text{vir}} \simeq 10^{12} h^{-1} M_{\odot}$), λ_{gal} decreases, f_{gas} decreases and $C_{\text{S}2\text{s}}$ increases, and the inner rotation curve becomes dominated by baryons. Adiabatic contraction increases the density of the halo, especially in the inner few percent of the virial radius. The differences between models with and without adiabatic contraction are in general small, with the exception of the amplitude of the inner rotation curve. See text for further details.

produce galaxies with realistic mass fractions $\lesssim 33\%$, mass outflows (i.e. feedback) are required.

The effect of feedback on the surface density profiles is shown in Fig. 2. The upper panels show a model with the SS05 AMD and $\alpha = 0.90$ and with the feedback efficiency varying from left to right: $\epsilon_{\text{EFB}} = 0.00, 0.10, 0.25, 0.50$, and 1.00 . The lower panels show a model with $\epsilon_{\text{EFB}} = 0.25$, and the SS05 AMD varied over the 2σ range as in Fig. 1 (this corresponds to model III in DB08).

Feedback effects the surface density profile in two ways: 1) it removes mass, decreasing the galaxy mass fraction, and 2) it preferentially removes low angular momentum material which also modifies the AMD. The galaxy mass fractions, $m_{\text{gal}} = M_{\text{gal}}/M_{\text{vir}}$ (defined as the ratio between the galaxy mass and the total mass of the galaxy-halo system), and galaxy spin parameters, $\lambda_{\text{gal}} = (j_{\text{gal}}/m_{\text{gal}})\lambda$, (where

$j_{\text{gal}} = J_{\text{gal}}/J_{\text{vir}}$ is the ratio between the total angular momentum of the galaxy and that of the galaxy-halo system) are given for each model. As the feedback efficiency is increased the galaxy mass fraction decreases and the galaxy spin parameter increases (upper panels of Fig. 2). Both of these result in a more extended disk and a more gradually rising rotation curve. By decreasing the amplitude of the rotation curve at small radii gas will settle in centrifugal equilibrium at a larger radius, hence resulting in a less concentrated disk. Feedback also preferentially removes low angular momentum material, which also directly results in a less concentrated disk.

In these models the halo was uncontracted (as models with halo contraction over-predict the zero point of the TF relation). Halo contraction would make the trends with feedback efficiency stronger, as high galaxy mass fractions

will result in more halo contraction, higher circular velocities and hence higher stellar central densities.

The amount of gas ejected as a function of radius depends on both the star formation rate and the depth of the potential well. Since both star formation is more efficient and the potential well is deeper in the centers of galaxies it is not obvious which effect should dominate. Indeed, as shown in DB08, globally, the depth of the potential well dominates over the star formation efficiency, such that galaxies in less massive haloes eject a higher fraction of their accreted gas. However, locally, for a fixed halo mass, smaller (i.e. lower spin parameter) galaxies are more efficient at removing their baryons, because the higher star formation rates are more than enough to compensate for the deeper potential well.

The lower panels of Fig. 2 show the effect of variation in the AMD shape parameter, α , over the 2σ range as found in cosmological simulations. These models can be compared with those in the lower panels of Fig. 1, where the galaxy mass fractions and spin parameters were fixed at $m_{\text{gal}} = 0.058$ and $\lambda_{\text{gal}} = 0.028$ respectively. In Fig. 2 the galaxy mass fractions and spin parameters are determined by the efficiencies of feedback and cooling. Qualitatively the surface density profiles and circular velocity profiles are similar between the two models. However, there are some small differences which highlight the impact the distribution of the baryons have in determining the amount of mass that can be removed. Larger values of α result in lower galaxy mass fractions (i.e. feedback is more efficient). This is a direct result of the shallower potential well created by a less concentrated baryonic disk, which makes it easier to eject baryons from the center of the galaxy. For the model with $\alpha = 1.48$, a comparison between Fig. 1 and Fig. 2 shows that feedback has removed the ‘‘bulge’’ component, creating a hollow core in the disk density profile. This results in a stellar disk less concentrated than exponential. On the other hand, for low values of α , there is more low angular momentum material, which results in a deeper potential well, from which it is harder to remove gas.

3.4 The Role of Halo Mass

Having discussed the effects of the AMD and feedback efficiency on the surface density profiles for a single halo mass, with median concentration and spin parameters, we now turn our attention to halo mass dependence of galaxy surface density profiles. Fig. 3 shows the surface density and circular velocity profiles for 5 model galaxies with $\log(M_{\text{vir}}/[h^{-1}M_{\odot}]) = 10.0, 11.0, 11.5, 12.0,$ and 13.0 . All of these models have the same halo angular momentum parameters: $\alpha = 0.90$, $\lambda = 0.025$, yet their resulting galaxy spin parameters, λ_{gal} , and stellar concentrations, C_{82s} , vary systematically with halo mass. Below a halo mass of $M_{\text{vir}} = 10^{12}M_{\odot}$ almost all of the baryons that accrete onto the halo have had time to cool, so the differences between the structural properties of the galaxies are a result of the efficiency at which feedback can remove mass and angular momentum from the disk and halo. As shown in DB08, mass loss is more efficient from lower mass haloes, and thus feedback has a larger impact on the density profiles of low mass galaxies. Since star formation is biased to small radii (due to the density dependence of the star formation rate), the mass that gets removed has lower than average specific angular mo-

mentum. The ejection of low angular momentum material directly lowers the concentration of the stars. The reduced galaxy mass fractions and higher galaxy specific angular momentum result in a more dark matter dominated circular velocity profile.

In massive haloes, $M_{\text{vir}} \simeq 10^{13}h^{-1}M_{\odot}$ feedback is inefficient at removing mass. Cooling is also inefficient, which results in a low galaxy mass fraction, $m_{\text{gal}} = 0.033$. But because cooling occurs from the inside out, the resulting spin parameter of the galaxy is very small, $\lambda_{\text{gal}} = 0.008$. Thus the resulting galaxy is very compact and concentrated, which resembles early type galaxies more than late type galaxies. However, we do not consider these models to be realistic, as the effects of mergers and secular evolution (which are not taken into account in our models) are likely to play a significant role in producing bulges in high mass haloes.

3.5 The Role of Adiabatic Contraction

The lower panels of Fig. 3 show the same models as the upper panels but including the effect of adiabatic contraction. Adiabatic contraction increases the density of the dark matter halo (red lines in Fig. 3) in the inner 10% of the virial radius. A deeper potential well results in a higher escape velocity, and thus mass ejection is less efficient. As shown in Fig. 3 and as discussed in Dutton & van den Bosch (2008), models with adiabatic contraction have higher rotation velocities and smaller sizes than models without adiabatic contraction. As might be expected the effect on the density profile of the disk is to increase its concentration, but the effects are in general small, especially in low mass haloes. Thus adiabatic contraction does not play a significant role in determining the density profiles of galaxy disks.

3.6 The Role of Stellar Populations

Fig. 4 shows surface brightness profiles in K-, I- and B-bands of the models in the lower panels of Fig. 2 (varying AMD shape) and the upper panels of Fig. 3 (varying halo mass). In each panel the concentration parameter, C_{82s} , in K-, I-, and B-band light as well as in stellar mass is given. Concentrations are largest in stellar mass and smallest in B-band light. The differences depend both on the concentration of the stars and the mass of the galaxy, with differences typically a factor of $\simeq 1.4$. These differences are caused by color gradients: inner disks being redder than outer disks. The color gradients are a reflection of the inside-out formation of stellar disks, both because our star formation law results in more efficient star formation at higher gas densities (which occur at smaller radii), and because the gas disk is growing with time which reflects the growth of the dark matter halo. It is interesting to note that there are non-negligible differences between concentrations in K-band light and stellar mass, which we return to in §§ 4.2 & 5.3.

Fig. 4 also shows the exponential disk fits as dashed lines. The scale lengths in stellar mass, K-, I-, and B-band light are given for each model. The scale lengths in B-band lights are typically 1.14 times larger than those in I-band light, and 1.25 times larger than those in K-band light. Observationally, for nearby disk galaxies, MacArthur et al. (2003) finds a mean ratio of B-band to R-band scale

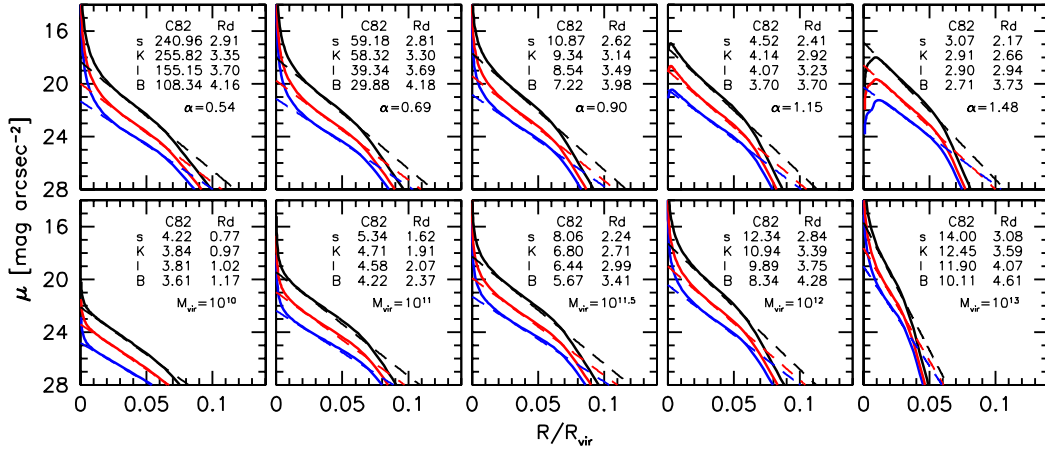


Figure 4. Effect of stellar populations on concentration index and disk scale lengths for model galaxies in the lower panels of Fig. 2 and upper panels of Fig. 3. For each model the surface brightness profiles in B-band (blue), I-band (red) and K-band (black) light are shown. The dashed lines show the exponential disk fits. The concentration parameters (defined as the ratio between radii enclosing 80 and 20% of the light (or stellar mass) and disk scalelengths) are given for each model.

lengths of $R_{d,B}/R_{d,R} = 1.15$, with a standard deviation of 0.15, and B-band to H-band scale lengths of $R_{d,B}/R_{d,H} = 1.34$ with a standard deviation of 0.20. Our models are consistent with these observations. If we also consider that extinction will most likely cause the observed gradients to be over-estimated, this will bring the models into even better agreement with the observations.

K-band light is generally considered a good tracer of stellar mass, but in our models the scale length of the K-band light is typically 1.2 times larger than the scale length in stellar mass. This also means that the scale lengths in B-band light are typically 1.5 times larger than those in stellar mass. Thus in order to derive stellar mass scale lengths (which are a fundamental parameter of disk galaxies) from observations, it is necessary to take into account the color gradients which will result in stellar mass-to-light ratio gradients, even in the near IR.

4 HOW COMMON ARE BULGE-LESS EXPONENTIAL DISKS?

We have shown that it is possible to produce quasi-exponential disks with Λ CDM initial conditions. However, these galaxies are not typical (in the sense they do not occur for median values of the input parameters) for any halo mass between 10^{11} and 10^{13} . However, in our models, low mass haloes produce disks with closer to exponential stellar profiles. Thus, an important observational question is to determine what fraction of galaxies, and late-type galaxies in particular, have bulge-less exponential disks and low bulge fractions, as a function of stellar mass.

It is generally thought that bulge-less disk galaxies are fairly common, and as such, this presents a challenge to hierarchical galaxy formation models. This is especially the case if a significant fraction of galaxy bulges were formed via secular processes (e.g. Kormendy & Fisher 2005). Such

a conclusion is supported by recent analyses that find bulge-less disk galaxy fractions of 15% for a sample of edge-on disk galaxies (Kautsch et al. 2006), and $\sim 20\%$ for sample of visually classified quasi-bulge-less galaxies (Barazza et al. 2008). However, these analyses do not consider any mass dependence to the fraction of bulge-less galaxies, which may lead one to over predict the frequency of massive bulge-less galaxies.

In an attempt to get at least a preliminary (if not a definitive) answer to the question of how common are exponential bulge-less disks (as a function of stellar mass) we make use of Sérsic indices from the publicly available low redshift New York University Value Added Catalog (NYU-VAGC, Blanton et al. 2005). The low- z NYU-VAGC is based on the second data release of the SDSS (Abazajian et al. 2004), and consists of 28089 galaxies at distances of 10-200 Mpc ($0.0033 < z < 0.05$), which have been determined by correcting for peculiar velocities.

The Sérsic profile is given by

$$\Sigma(R) = \Sigma_0 \exp[-(R/R_s)^{1/n}], \quad (18)$$

where Σ_0 is the central surface density, R_s is the scale radius, and n is the Sérsic index. For $n = 4$ this profile corresponds to a de Vaucouleurs profile (de Vaucouleurs 1959), for $n = 1$ to an exponential profile, and for $n = 0.5$ to a gaussian. The NYU-VAGC provides Sérsic indices measured in each of the five SDSS pass-bands: *ugriz*. The Sérsic fits are performed with circular apertures, and thus are likely to given erroneous results for highly inclined disks. Furthermore, the surface brightness profiles of highly inclined disks are often strongly affected by extinction, so we wish to remove inclined disks remove from our sample. To do this we use the axis ratios measured from exponential fits (taken from the main SDSS catalog), and remove galaxies with axis ratios smaller than $b/a = 0.5$ (i.e. corresponding to an inclination of $\simeq 60^\circ$). This removes about half the galaxies in the sample. De Vaucouleurs fit axis ratios are also available, but

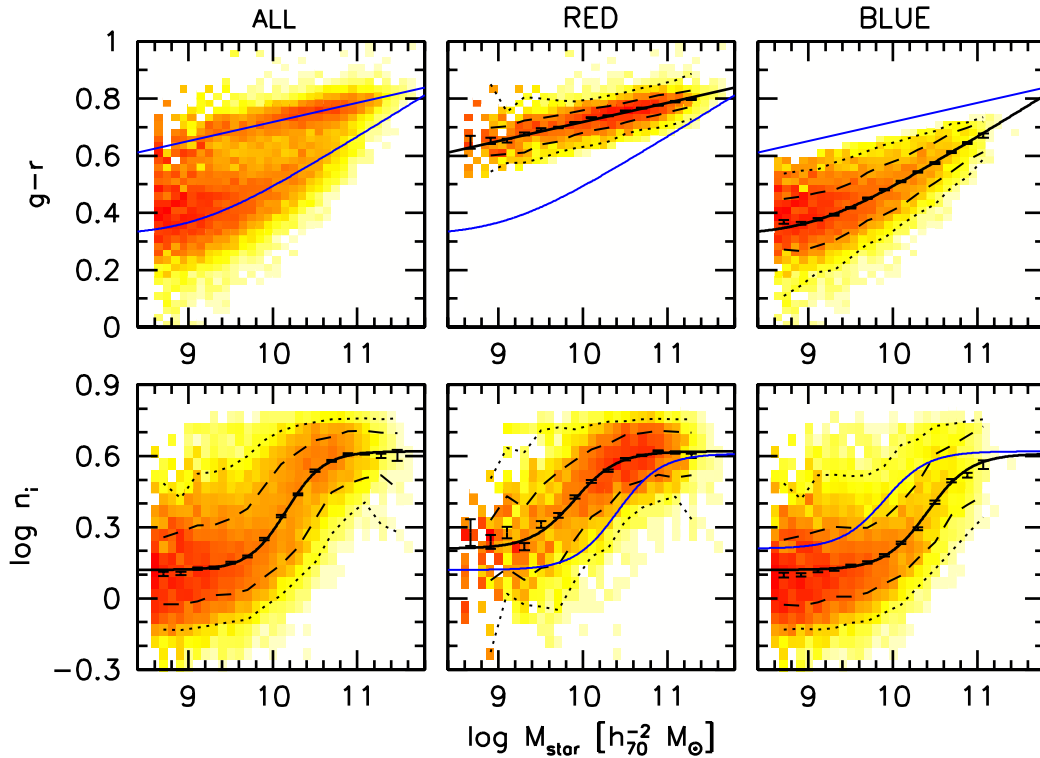


Figure 5. Color-stellar mass and Sérsic index-stellar mass relations for galaxies in the low redshift NYU-VAGC. The color coding corresponds to the relative number of galaxies in each bin, weighted by $1/V_{\max}$, on a logarithmic scale. Galaxies are selected to have stellar mass $M_{\text{star}} > 10^{8.6} M_{\odot}$, redshift $0.005 < z < 0.05$, and axis ratio $b/a > 0.5$. We separate galaxies into red (middle) and blue (right) according to their position in the $u - r$ color- r magnitude diagram, using the relation in Baldry et al. (2004). In addition we require that red galaxies are not bluer than 0.1 dex from the red sequence, and that blue galaxies are at least 0.05 dex bluer than the red sequence. We show the median (solid), 15.9th and 84.1th (dashed), 2.3th and 97.7th (dotted) percentiles of the distributions of color and Sérsic index in stellar mass bins of width 0.2 dex. The error bars show the Poisson error on the median. The thick solid lines show fits to the median relations, see Table 1 for fit parameters. For the red galaxies we show the relations for the blue galaxies as thin solid lines, and vice versa for the blue galaxies.

these often give axis ratios more representative of the bulge or bar, rather than the disk, so they are not considered useful for our purposes.

For both Sérsic index and axis ratio we adopt the i -band fits as this provides a trade off between signal to noise and wavelength. We calculate stellar masses using the relation between $g - r$ color and stellar mass-to-light ratio from Bell et al. (2003), with an offset of -0.1 dex corresponding to a Chabrier (2003) IMF:

$$\log M_{\text{star}}/L_r = -0.406 + 1.097(g - r) \quad (19)$$

The upper panels in Fig. 5 show the relation between color and stellar mass. We separate galaxies into red and blue galaxies using $u - r$ colors following Baldry et al. (2004), who determine the optimal color separation between red and blue galaxies to be

$$(u - r)_{\text{div}} = 2.06 - 0.244 \tanh\left(\frac{M_r + 20.07}{1.09}\right), \quad (20)$$

where M_r is the r -band magnitude of the galaxy. In addition, to keep the red-sequence and blue-cloud “pure” in the $g - r$ vs M_{star} plane, we require that red galaxies are not bluer than 0.1 dex from the red-sequence, and that blue galaxies are at least 0.05 dex bluer than the red-sequence. The color-

mass relations for red and blue galaxies are shown in the upper middle and upper right panels respectively.

The lower panels in Fig. 5 show the relations between Sérsic index (measured in the i -band) and stellar mass. For all galaxies (left panel) the Sérsic index also shows a bi-modality, with a cloud of points at high masses around $n = 4$, and at low masses around $n = 1.3$. There is a rapid transition in Sérsic index between a stellar mass of $M_{\text{star}} = 1 \times 10^{10}$ to $5 \times 10^{10} M_{\odot}$. It is tempting to associate this bi-modality with the color bi-modality. However, if we look at early and late-types separately, we see the same trends: low mass galaxies have low Sérsic index and high mass galaxies have high Sérsic index. We return to the correlation between color and Sérsic index in § 4.2 below.

In order to calculate residuals, and to ease comparisons with models we fit the relations in Fig. 5 with the following. We fit the color-mass relation of the red galaxies with a single power-law

$$(g - r) = (g - r)_0 + \log\left(\frac{M_{\text{star}}}{M_0}\right)^{\alpha}. \quad (21)$$

We fit the color-mass relation of the blue galaxies with a double power-law

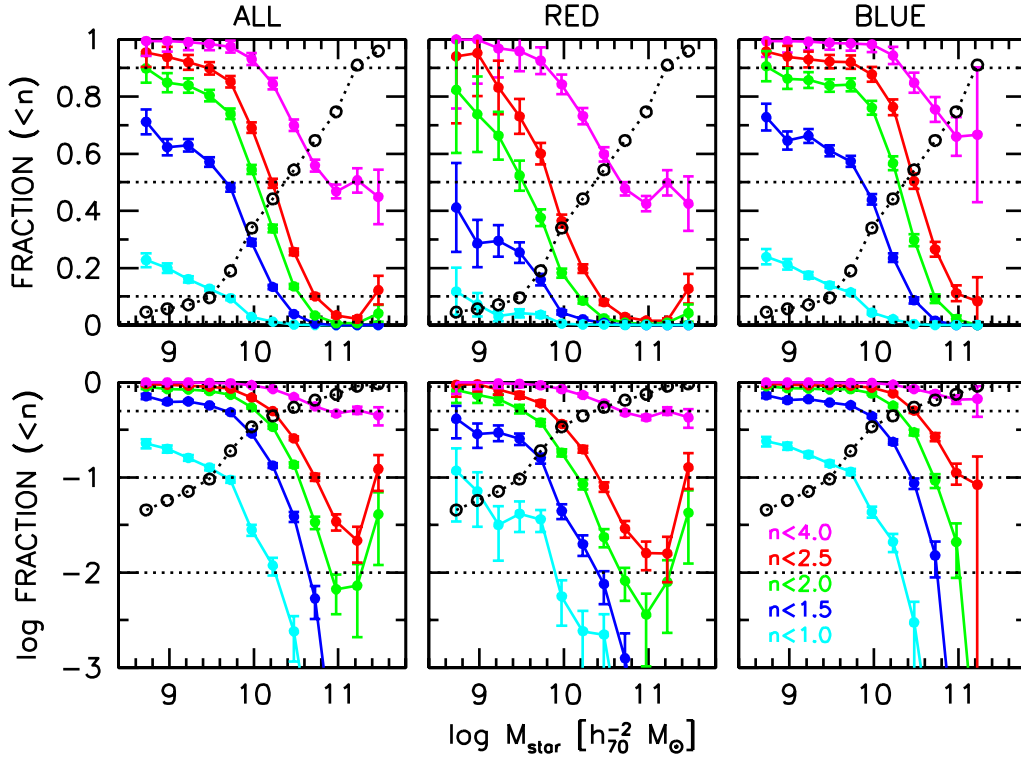


Figure 6. Fraction of galaxies at a given stellar mass with Sérsic index less than 1.0 (cyan), 1.5 (blue), 2.0 (green), 2.5 (red), and 4.0 (magenta). The left panels show results for all galaxies, middle panels for red galaxies, and the right panels for blue galaxies. The black points show the fraction of red galaxies at a given stellar mass. The upper panels show the fractions in linear space. The lower panels show the fractions in log-space, which highlights the scarcity of bulge-less galaxies (i.e. low n) at high masses.

Table 1. Best fit parameters for median color-mass and Sérsic-mass relations from Fig. 5 using the functions in Eqs. (21-23).

Sample	$\log M_0$	$(g-r)_0$	α	
RED	10.00	0.718	0.067	
Sample	$\log M_0$	$(g-r)_0$	α	β
BLUE	9.10	0.375	0.00	0.182
Sample	$\log M_0$	$\log n_1$	$\log n_2$	γ
ALL	10.16	0.12	0.62	1.95
RED	9.90	0.21	0.62	1.70
BLUE	10.41	0.12	0.61	1.70

$$(g-r) = (g-r)_0 + \log \left(\frac{M_{\text{star}}}{M_0} \right)^\alpha + \log \left(\frac{M_0 + M_{\text{star}}}{2M_0} \right)^{\beta-\alpha}. \quad (22)$$

We fit the Sérsic index - stellar mass relations with the following function:

$$\log n = \log n_2 + \frac{(n_1 - n_2)}{1 + 10^{\gamma \log(M_{\text{star}}/M_0)}}. \quad (23)$$

Here n_1 is the asymptotic value of n at low mass, n_2 is the asymptotic value of n at high mass, M_0 is the transition mass, and γ controls the sharpness of the transition. The best fit parameters are given in table 1.

From Fig.5 it is apparent that massive galaxies with low

Sérsic indices are rare, both for red and blue sub-samples. To be more quantitative Fig. 6 shows the fraction of galaxies at a given stellar mass with Sérsic index less than 1.0 (cyan), 1.5 (blue), 2.0 (green), 2.5 (red), and 4.0 (magenta). Also shown is the fraction of all galaxies that are red (black dotted). The red-galaxy fraction steadily increases from low to high stellar mass. Note that our red galaxy fraction is biased high due to our axis ratio cut, which preferentially removes disk (and hence typically blue) galaxies.

At the transition mass of $2.5 \times 10^{10} M_\odot$ the median Sérsic index of the late types is $n \simeq 2$. We adopt a Sérsic index of $n = 1.5$ as an upper-limit on the Sérsic index of a bulge-less galaxy (which was also the definition used by Bell 2008). Thus at the transition mass, less than $\simeq 15\%$ of blue galaxies are bulge-less. At higher masses the bulge-less galaxy fraction drops rapidly. To show just how rare massive bulge-less galaxies are, the lower panels show the fractions on a logarithmic scale.

Using the TF relations from Pizagno et al. (2005) and Dutton et al. (2007), galaxies with rotation velocities of 220 km s^{-1} (e.g. such as the Milky-Way) have a median stellar mass of $M_{\text{star}} \simeq 10^{11} M_\odot$. Note that the actual stellar mass of the Milky-Way is thought to be $\simeq 5 \times 10^{10} M_\odot$ (Widrow, Pym & Dubinski 2008), which means that the Milky-Way does not fall on the TF relation (Hammer et al. 2007). These galaxies have a median Sérsic index of $n \simeq 3.5$, and less than 0.1% of these galaxies are bulge-less (i.e. have $n < 1.5$).

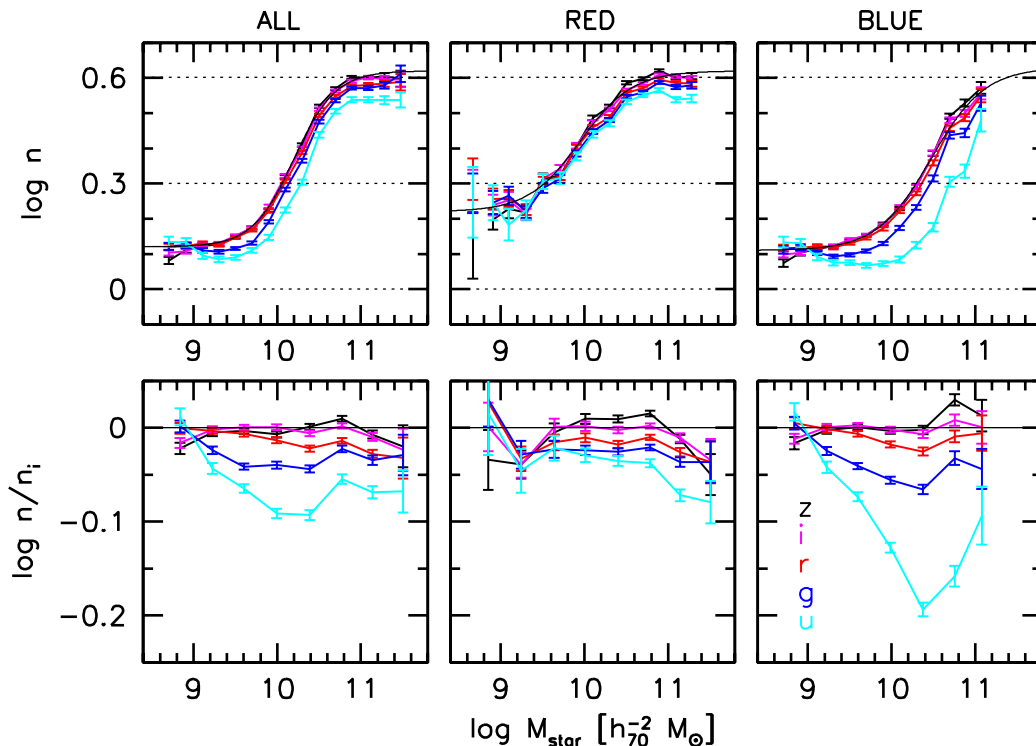


Figure 7. Dependence of Sérsic index on pass-band. The upper panels show the median Sérsic index - stellar mass relation for Sérsic index measured in each of the five SDSS pass-bands: u , g , r , i , and z . The lower panels show the deviation of the Sérsic index measured in the u , g , r , and z bands relative to that measured in the i band. The dependence of Sérsic index on wavelength is strongest for blue galaxies, and peaks at the transition mass of $M_{\text{star}} \simeq 2.5 \times 10^{10} M_{\odot}$.

This provides some relief for theorists who have been trying unsuccessfully to produce a bulge-less Milky-Way mass galaxy (e.g. Abadi et al. 2003; Robertson et al. 2004; Governato et al. 2004; 2007). A more serious challenge for theorists is to produce galaxies like M33, as the majority of galaxies at these masses do not have significant bulges. For a galaxy like M33, with a rotation velocity of 120 km s^{-1} and a stellar mass of $1 \times 10^{10} M_{\odot}$, the median $n \simeq 1.6$ and 45% of blue galaxies have $n < 1.5$. This means that quasi-bulgeless galaxies are the norm in low mass galaxies, which means they must form in dark matter haloes with typical mass accretion histories. Thus if cosmological simulations fail to produce galaxies like M33, this signals a failure of the model, and not an unfortunate choice of mass accretion history. By contrast, since massive disk dominated galaxies, such as the Milky-Way (which has a bulge fraction of $\simeq 0.2$ (Widrow, Pym & Dubinski 2008) are rare, they may have formed in haloes with a very unusual mass accretion histories. This makes simulating the Milky-Way a harder problem, because it would take a sample of hundreds of Milky-Way mass haloes before one would expect to produce a galaxy resembling the Milky-Way.

4.1 The Wavelength Dependence of the Sérsic Index

In Fig. 7 we show the median Sérsic index - stellar mass relation for the Sérsic index measured in each of the 5 SDSS pass-bands $ugriz$. The general trend is for lower Sérsic in-

dexes in bluer pass bands. This is true for both red and blue galaxies, but the effects are strongest for the blue galaxies. This could be attributed to the greater sensitivity of bluer pass-bands to extinction and/or variations in the star formation history as a function of galacto centric radius. The lower panels of Fig. 7 show the differences between the Sérsic index as measured in the u , g , r , and z -bands to that measured in the i -band. The largest differences occur around the transition mass of $2.5 \times 10^{10} M_{\odot}$.

These results have implications for studies of galaxy structure at high redshift. Currently large surveys with HST imaging, such as the Galaxy Evolution and Morphology Survey (GEMS) (Rix et al. 2004), the All-wavelength Extended Groth strop International Survey (AEGIS) (Davis et al. 2007), and the cosmological evolution survey (COSMOS) (Scoville et al. 2007; Koekemoer et al. 2007) are limited to the F814W or the F850LP filters (hereafter referred to as the $I814$ and $z850$ bands). At redshift $z = 1$ the $I814$ filter shifts into the U -band, while the $z850$ filter corresponds to B-band. In an attempt to make a fair comparison between galaxies at different redshifts, authors often compare structural properties in the rest frame B or V bands at low and high redshifts. However, given that these bands do not trace stellar mass even at low redshift, and that star formation rates at $z \simeq 1$ were an order of magnitude higher than they are today (e.g. Noeske et al. 2007), it is not clear that such a comparison gives an unbiased view of the evolution of galaxy structure in stellar mass. To determine the structural properties of galaxies at $z \gtrsim 1$ free of the biases of young

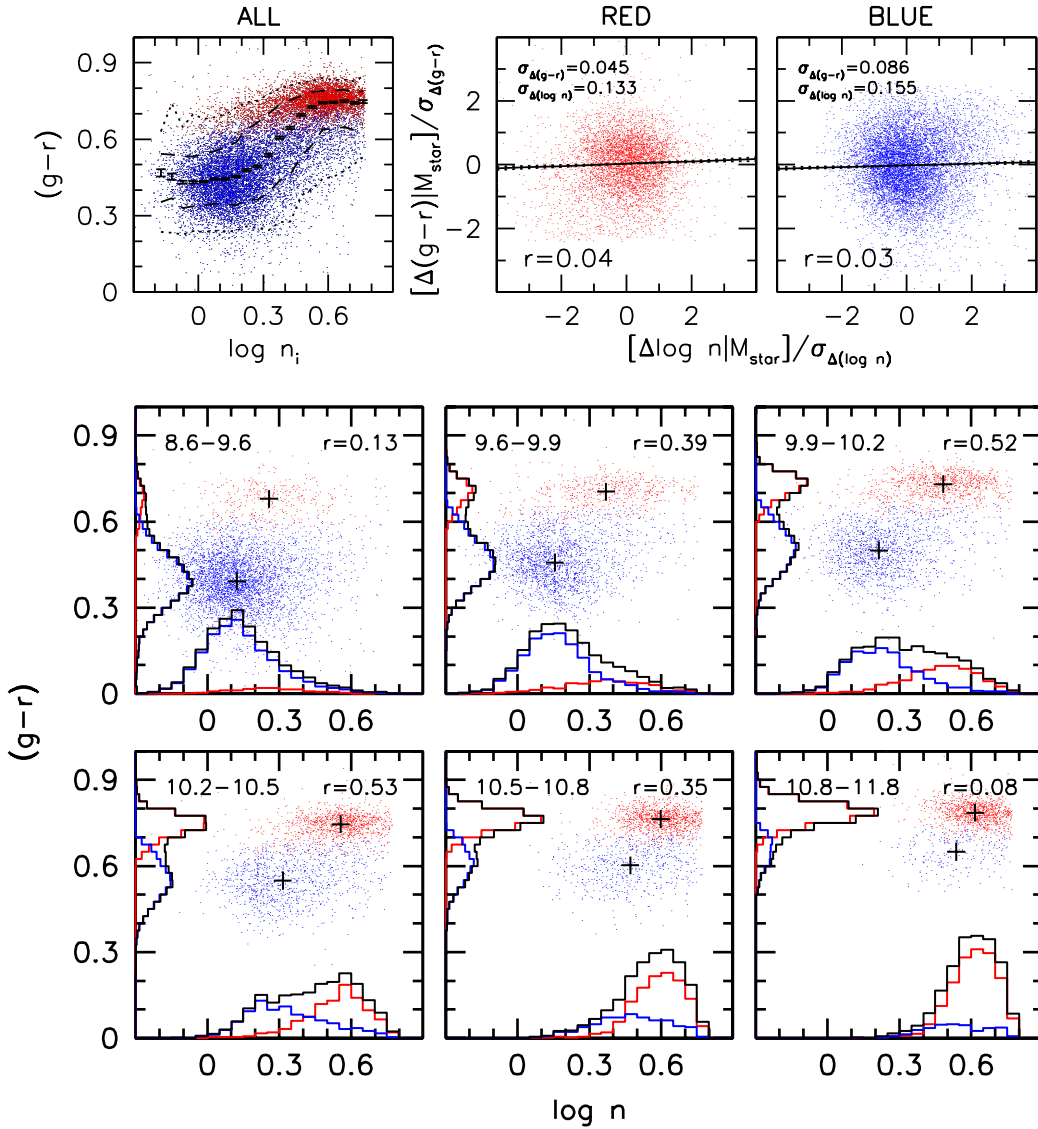


Figure 8. Correlations between color and Sérsic index. The upper left panel shows color vs Sérsic index for all galaxies in our sample, color coded by whether they are in the red sequence or blue cloud. This shows a clear correlation between color and Sérsic index. The upper right panels show the residuals of the color-mass relation versus the residuals of the Sérsic mass relation, both for red and blue galaxies. The solid lines show the best fit of Δ color vs Δ Sérsic index, with dashed lines indicating the error on the slope. The correlation coefficient, r , for each fit is also shown. This shows that within the blue cloud or red sequence, the scatter in color and Sérsic index, at a given stellar mass, are uncorrelated. The lower panels show the color-Sérsic relations for 6 mass bins. The range in $\log M_{\text{star}}/[h_{70}^{-2} M_{\odot}]$ for each bin is given in the top left corner of each panel. The correlation coefficient between color and Sérsic index is given in the top right corner of each panel. The median color and Sérsic index for each mass bin is indicated by a cross. This shows that whether a galaxy is red or blue does depend on its Sérsic index, especially near the transition mass of $M_{\text{star}} \simeq 2.5 \times 10^{10} M_{\odot}$.

stellar populations and dust will require high resolution NIR imaging, preferably in more than one band to provide rest frame red pass band and an optical color to correct for stellar population and extinction gradients within galaxies.

4.2 Is Sérsic Index Correlated with Color?

From Fig. 5 we see that higher mass galaxies are both redder and more concentrated than lower mass galaxies. Thus globally there is a correlation between Sérsic index and color: galaxies with lower Sérsic index are bluer; galaxies with

higher Sérsic index are redder. This correlation is shown in the upper left panel of Fig. 8. However, this does not mean that there is a causal relation between Sérsic index and color. The upper right panels of Fig. 8 show the residuals of the color-mass relation vs. the residuals of the Sérsic-mass relation. For both red and blue galaxies the correlation is consistent with zero, i.e. within the blue cloud or red-sequence, the scatter in color, at a given stellar mass, is uncorrelated with the scatter in Sérsic index. How do we reconcile this fact with the strong global correlation between Sérsic index and color?

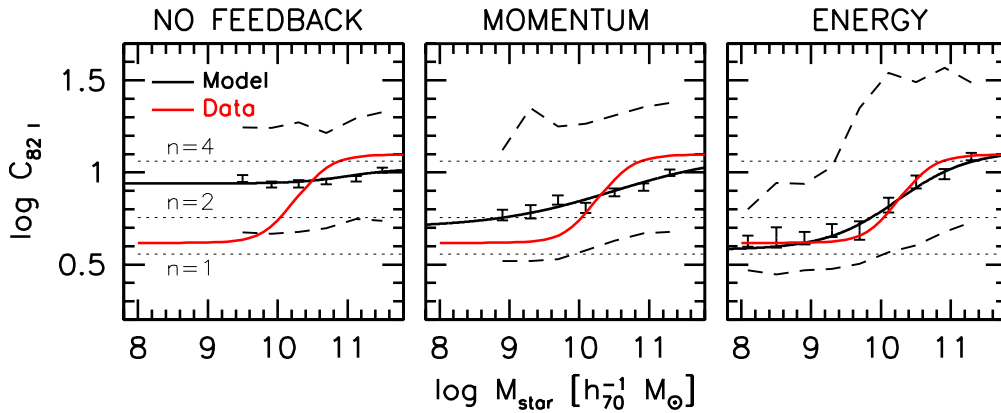


Figure 9. Concentration of the I-band light versus stellar mass for three feedback models. The black lines show the 16th, and 84th percentiles (dashed), and a fit to the median values (solid). The red line shows the median relation for the observations (from Fig. 5 after converting from Sérsic index to concentration). The dotted lines show, for reference, the concentration corresponding to a Sérsic index of $n = 1, 2$, and 4 . The energy driven feedback model produces disk galaxies that have Sérsic indices that are in good agreement with the observations.

The middle and lower panels of Fig. 8 show the color-Sérsic relation for 6 mass bins from $M_{\text{star}} = 10^{8.6}$ to $10^{11.8} M_{\odot}$. This shows that at a given stellar mass whether a galaxy is blue or red does depend on its Sérsic index, especially near the transition mass of $2.5 \times 10^{10} M_{\odot}$. Galaxies with high Sérsic indices are more likely to be on the red-sequence than in the blue cloud. This result is consistent with Bell (2008), who showed that having a bulge is a requirement for a central galaxy being on the red-sequence, which is a central prediction of AGN feedback scenarios for quenching star formation.

5 COMPARISON BETWEEN MODELS AND OBSERVATIONS

Having established observationally that Sérsic index is a strong function of stellar mass, we now investigate whether our models can reproduce this trend. We consider three models with different feedback prescriptions: 1) no feedback; 2) momentum driven feedback; and 3) energy driven feedback. The parameters of these models are given in Table 2. For each model we generate Monte Carlo samples with halo masses ranging from $10^{10} < M_{\text{vir}} < 10^{13} h^{-1} M_{\odot}$, corresponding to virial velocities ranging from $31 \lesssim V_{\text{vir}} \lesssim 310 \text{ km s}^{-1}$. We also include log-normal scatter in the halo concentration, c , halo spin parameter, λ , and halo angular momentum shape parameter, α . The scaling relations of these models are discussed in more detail in DB08.

5.1 Concentration Mass Relation

The upper panels of Fig. 9 shows the concentration of the I-band light as a function of stellar mass for these three models. Recall that we define the concentration parameter as the ratio between the radii enclosing 80 and 20% of the I-band light: $C_{82I} = R_{80I}/R_{20I}$.

The model without feedback results in a median concentration of $\simeq 9$, which corresponds to a Sérsic index of $\simeq 3.5$. The high concentrations are a result of the high galaxy mass

Table 2. Model Parameters

Name	ϵ_{EFB}	ϵ_{MFB}	$\bar{\lambda}$	$\sigma_{\ln \lambda}$	AC
I: No Feedback:	0.0	0.0	0.035	0.35	N
II: Momentum:	0.0	1.0	0.035	0.35	N
III: Energy:	0.25	0.0	0.025	0.35	N

fractions, which cause the baryons to dominate the inner circular velocity profile. The model with momentum driven wind also results high concentrations at high stellar masses $M_{\text{star}} \simeq 10^{11} M_{\odot}$, but also shows a trend of decreasing concentration with decreasing stellar mass, in qualitative agreement with the observations (solid red line). However, the observed relation has a sharper transition, as well as both lower concentrations at low masses and higher concentrations at high masses. The energy driven wind model results in a much better agreement with the observed relation. It has the correct asymptotic values for the concentrations at both low and high masses. In particular this model successfully produces galaxies with close to exponential surface brightness profiles at low stellar masses. We emphasize that none of these models have been tuned to reproduce the concentration mass data. The feedback efficiencies of these models were chosen so that the models reproduce the zero points of the TF and size-stellar mass relations (see DB08).

5.2 Scatter in Concentrations

In all three models there is a significant scatter in the concentration index at a given stellar mass. To determine where this scatter comes from we show in Fig. 10 the concentration-mass relation for the energy driven feedback model where there is only one source of scatter: c , λ , or α . This shows that the scatter in the I-band concentration-stellar mass relation is dominated by the angular momentum shape parameter, with the halo spin parameter contributing some scatter, and halo concentration resulting in a negligible amount of scatter. Note also that the scatter in concentrations depends on

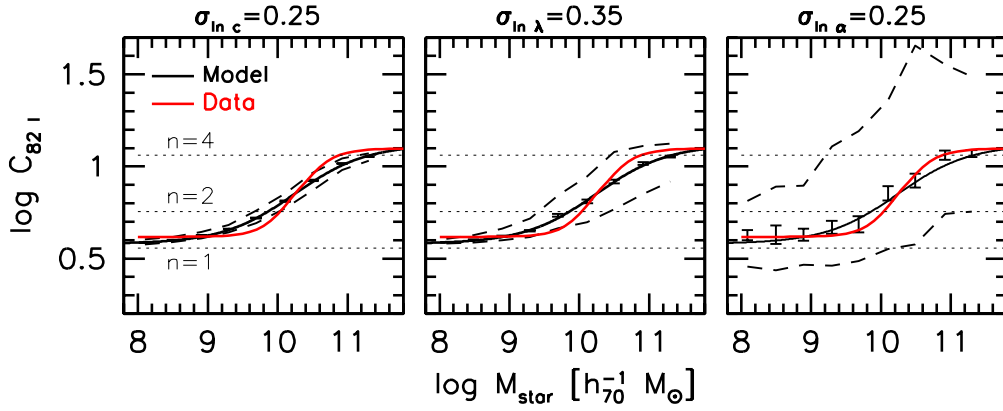


Figure 10. Concentration-mass relation for the energy feedback model for three different sources of scatter: c (left); λ (middle) and α (right). The scatter in the concentration mass relation is dominated by scatter in α , the angular momentum shape parameter. The lines are as in Fig 9.

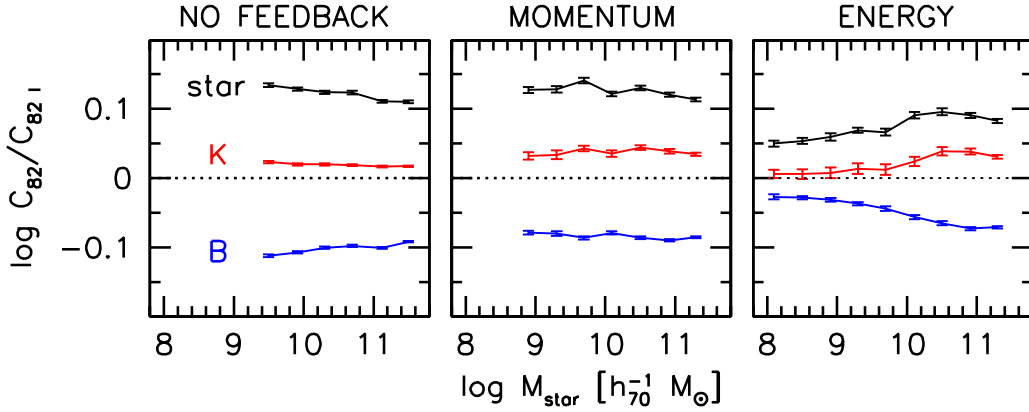


Figure 11. Difference between concentration measured in I-band to that measured in stellar mass (black), K-band light (red) and B-band light (blue), vs stellar mass. The energy driven feedback model produces disk galaxies that have color gradients that are in good agreement with the observations.

stellar mass, with less scatter at lower masses. This shows that feedback is able to, at least partially, erase the initial conditions.

The scatter in the concentration mass relation in the models is significantly larger, by at least a factor of two, than in the observations. In Fig. 1 we saw that the SS05 AMD results in larger scatter in disk concentration than the B01 AMD. Thus an important question for theorists is to determine in detail the range of AMD's of dark matter and gas in cosmological simulations.

5.3 Differences Between Concentrations in Stellar Mass and Light

Fig.11 shows the differences, with respect to the I-band light, of the concentration indices measured in the stellar mass (black lines), K-band light (red lines) and B-band light (blue lines). As might be expected, in all three models the concentrations are highest in stellar mass, and lowest in B-band light. As discussed in § 3.6 the color gradients are a reflection of the inside-out formation of stellar disks. However, what

may be surprising is that the K-band concentrations are not equal to those of the stellar mass. Furthermore, the difference between I-band and stellar mass is about the same as that between B-band and I-band. This suggests that an accurate determination of the concentration of the stellar mass in disk galaxies requires the color gradients (and hence stellar mass-to-light gradients) to be taken into account.

In the observations, low mass galaxies, $M_{\text{star}} \simeq 10^9 M_{\odot}$, have small differences between Sérsic indices in different pass bands. The differences between Sérsic indices in different pass bands increase with stellar mass, reaching a maximum at around the transition mass of $2.5 \times 10^{10} M_{\odot}$. Qualitatively similar trends of light concentration with stellar mass are found with our energy feedback model. The momentum feedback and no feedback models, however, have almost no mass dependence to the concentrations, in clear conflict with the observations.

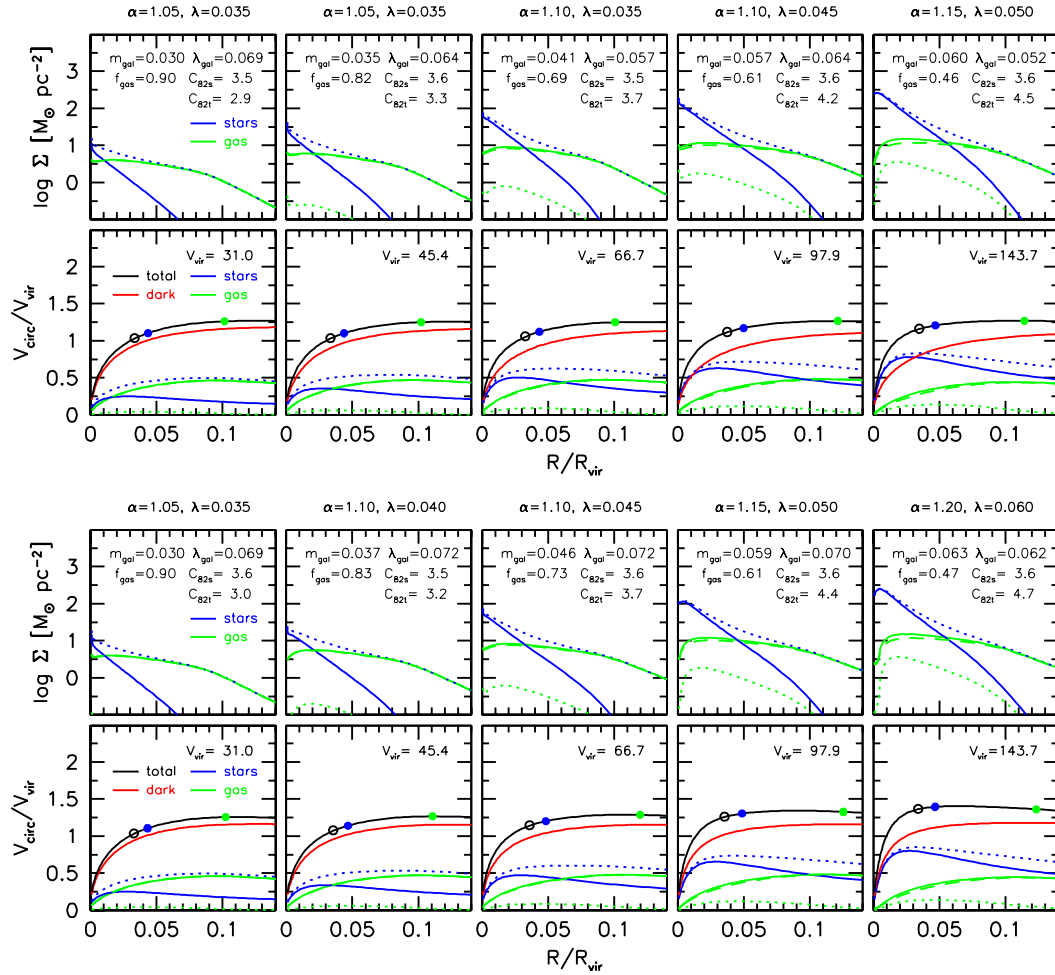


Figure 12. Examples of galaxies with exponential stellar density profiles (solid blue lines) in our energy driven feedback ($\epsilon_{\text{EFB}} = 0.25$) model. Virial mass increases left to right from $M_{\text{vir}} = 10^{10} h^{-1} M_{\odot}$ to $M_{\text{vir}} = 10^{12} h^{-1} M_{\odot}$. All models follow the concentration mass relation. The halo angular momentum parameters, α and λ , for each model are specific at the top of the surface density panels. These values are typically within 1σ of the values predicted from cosmological simulations. The models produce exponential stellar disks with (lower panels) and without (upper panels) adiabatic contraction. The line types and colors are the same as in Fig.1.

5.4 Examples of Model Exponential Stellar Disks

From the light concentration - stellar mass plots of Figs.9 & 10 it is apparent that galaxies with concentrations consistent with pure exponential surface brightness profiles are produced by our models with feedback, typically within the 1σ variations of the halo angular momentum parameters. In Fig.12 we show examples of such cases. These models have exponential stellar disks over the radial range of $\simeq 0$ to $\simeq 5$ stellar disk scale lengths. Virial mass increases left to right from $M_{\text{vir}} = 10^{10} h^{-1} M_{\odot}$ to $M_{\text{vir}} = 10^{12} h^{-1} M_{\odot}$. The halo angular momentum parameters (α, λ) of these models are specified above the surface density plots. For comparison, the median and 1σ upper scatter in these values in cosmological simulations are (0.90, 1.15) for α (Sharma & Steinmetz 2005) and (0.035, 0.60) for λ (Maccio et al. 2007). The upper panels are galaxies taken from Model III, while the lower panels are taken from an equivalent model but with adiabatic contraction of the halo. The models with adiabatic contraction also produce pure exponential stellar disks, albeit with slightly higher values of (α and λ). This demon-

strates that the ability of our outflow models to produce pure exponential stellar disks is not dependent on the effect of adiabatic contraction.

5.5 Are Outflows Needed to produce Exponential Stellar Disks?

We have shown that a model with SN driven mass outflows can reproduce the observed dependence of light concentration with stellar mass of spiral galaxies. In particular this model can produce pure exponential stellar disks over a wide range in halo masses ($M_{\text{vir}} = 10^{10} - 10^{12} h^{-1} M_{\odot}$). We now ask the question of whether this result requires mass outflows, or whether it could be achieved by a model in which the baryon fraction was regulated by another mechanism. In another words: Is getting the right amount of cold baryons in a galaxy sufficient to produce exponential stellar disks?

We test this hypothesis by running models with the same galaxy mass fraction at redshift zero as our exponential stellar disk models from Fig 12. We implement this in our model by turning off the cooling time calculation, and

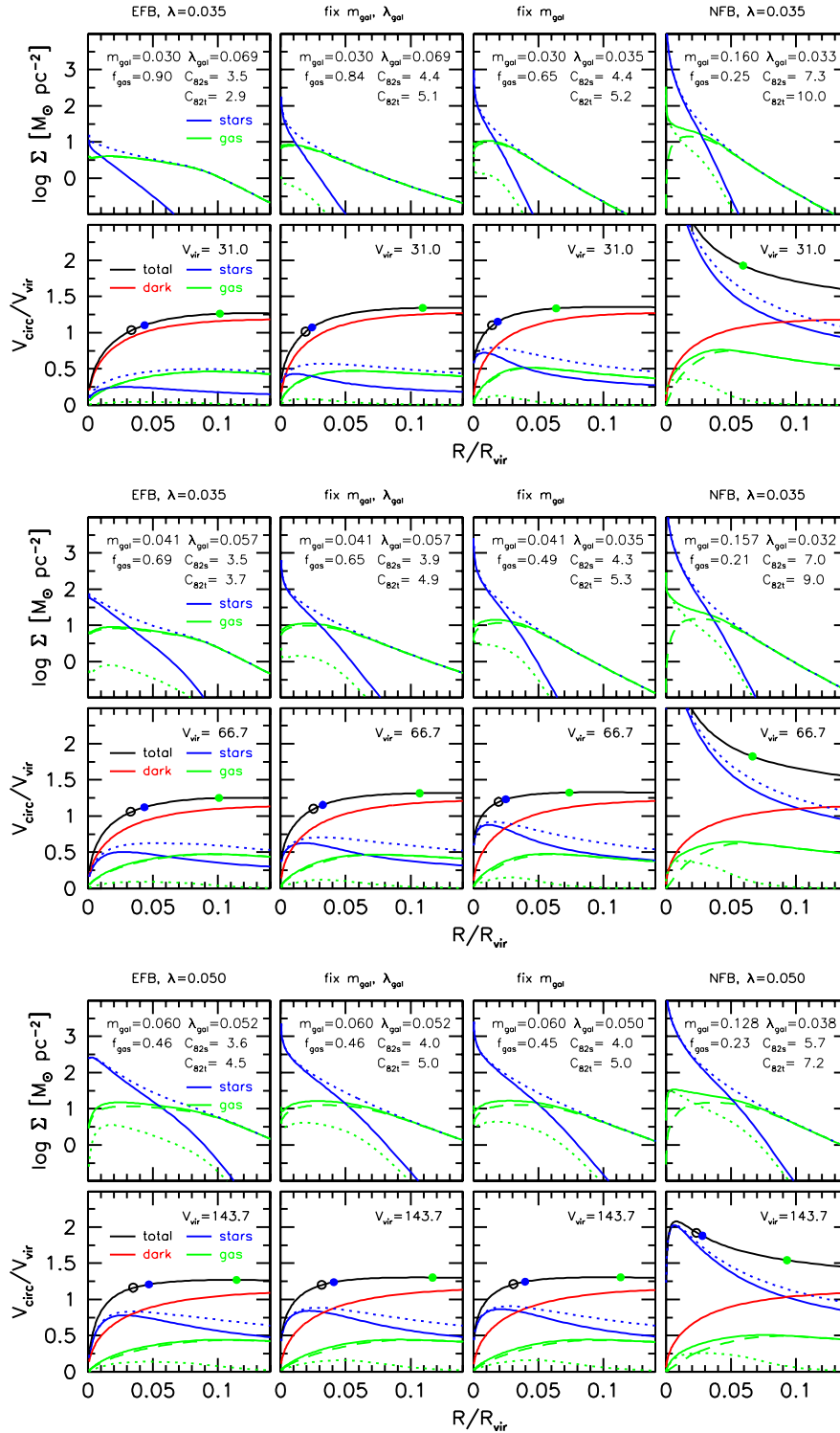


Figure 13. Feedback modifies the baryon fraction, total angular momentum and angular momentum distribution of the baryons. The models on the far left are the $M_{\text{vir}} = 10^{10} h^{-1} M_\odot$ (upper panels) and $M_{\text{vir}} = 10^{11} h^{-1} M_\odot$ (middle panels) and $M_{\text{vir}} = 10^{12} h^{-1} M_\odot$ (lower panels) models from Fig.12 (which were chosen to have exponential stellar disks). These models have energy driven feedback. The models second from the left have been constructed to have the same m_{gal} and λ_{gal} as the models on the far left. These models have different baryonic and stellar disk density profiles, with higher concentrations and smaller stellar disks in the models without feedback. This shows that feedback is modifying the angular momentum distribution. The models second from the right also have m_{gal} fixed to the value obtained with feedback, but has λ_{gal} fixed to the λ of the halo. The models on the far right have no feedback, and thus the m_{gal} and λ_{gal} are determined by the efficiency of cooling. These models have too many baryons, which results in disks that are too small, too concentrated, and with unrealistic rotation curves. See text for further details.

instead we set the amount of baryons that accrete onto the disk, at each time step, to be the desired galaxy mass fraction. The result is a model with our desired galaxy mass fraction as well as a galaxy spin parameter equal to the input halo spin parameter. We run this procedure for three halo masses: $M_{\text{vir}} = 10^{10}, 10^{11}, \& 10^{12} h^{-1} M_{\odot}$. The results of these test are shown in Fig. 13.

The models with feedback (and exponential stellar disks) are on the far left. Models with the same galaxy mass fractions and galaxy spin parameters (set by hand) are in the panels second from the left. These models have smaller disks with higher concentrations. This demonstrates that outflows have modified the distribution of angular momentum of the baryons relative to that of the dark matter. The models second from the right have galaxy mass fractions fixed to those of the models with feedback, but with galaxy spin parameters set equal to that of the dark matter. The models on the right have no feedback, and thus the m_{gal} and λ_{gal} are determined by the efficiency of cooling, which is close to 100% for these halo masses. These models have too many baryons, which results in disks that are too small, too concentrated, and with unrealistic rotation curves.

This sequence of models shows that getting the right amount of baryons into a galaxy is not sufficient to produce exponential stellar disks. Furthermore, getting the right amount of baryons and specific angular momentum is also not sufficient to produce exponential stellar disks. For the models to produce exponential stellar disks they need to get the right amount of baryons, specific angular momentum, and distribution of specific angular momentum. SN driven mass outflows are a mechanism that reduces galaxy mass fractions and at the same time naturally modifies the angular momentum distribution of the baryons in the desired way. It remains to be seen whether other mechanisms for reducing the baryon fraction of galaxies, can be found that also modify the angular momentum of baryons in the desired way.

6 DISCUSSION

6.1 Are Galaxy Disks Universally Exponential?

A common assumption in galaxy formation models, and observational bulge-to-disk decompositions is that disks are exponential. This is not without some motivation. 1) Galaxies that are observed to be bulge-less (i.e. they have no spheroid), invariably have close to exponential light profiles, NGC 300 is a example of a galaxy with an exponential stellar disk over 10 scale lengths (Bland-Hawthorn et al. 2005). 2) Even if a galaxy is not bulge-less, the disk is often well fitted by an exponential over several scale lengths, so it is tempting (especially when plotting surface intensity on a log-linear plot) to extrapolate the exponential disk to small radii, and to associate all of the excess light to a bulge. 3) Exponential profiles are also easy to work with analytically: mass profiles, and rotation curves can be computed easily. However, there are several reasons to question the assumption that stellar disks are universally exponential.

From a theoretical point of view, the formation of pure exponential disks is a mystery. It has been known since Messtel (1963) that a uniform sphere in solid body rotation has a

specific angular momentum distribution close to that of an exponential disk. But as shown by e.g. Dalcanton Spergel & Summers (1997), when a gas disk with a solid body AMD is in centrifugal equilibrium in an dark matter halo, the center of the disk is significantly more concentrated than an exponential, and there is an outer cut off at around 4 disk scale lengths.

Viscous evolution is often cited as a mechanism for explaining exponential disks (Olivier, Blumenthal, & Primack 1991; Ferguson & Clarke 2001; Bell 2002). However, it requires initial conditions that are less concentrated than exponential to start from, which in Λ CDM is *the* problem. Viscous process always increase the amount of mass at small radii, so even if it is a mechanism to explain why stellar disks are exponential over a large number of scale lengths, it does not explain the existence of bulge-less exponential disks.

Angular momentum distributions of baryons and dark matter in a Λ CDM cosmology are typically quite different from that required to produce exponential disks (Bullock et al. 2001b; Sharma & Steinmetz 2005). In particular, they tend to have too much low and high angular momentum material. The excess of high angular momentum material may not be a serious problem as at larger radii gas dominates over stars. In addition gas at large radii can be ionized making it hard to detect. The excess of low angular momentum material is considered the more serious problem.

We have shown that it is possible (through SN driven outflows and density dependent star formation) to make disk galaxies with realistic stellar surface brightness profiles with Λ CDM initial conditions. In many cases the disk is exponential over several scale lengths, but upturns above an exponential profile at small radii are ubiquitous. When present in observed galaxies, these upturns above an exponential, are generally considered to be due to a bulge or a pseudo-bulge. However, given that there is no theoretical motivation for the existence of pure exponential disks, it seems reasonable to suppose that in some cases these upturns are actually part of the disk. Such a conclusion has been reached before: quoting from Kormendy & Kennicutt 2004 “*We already accept Freeman 1970 Type II profiles as canonical disk behaviour, even though we can explain it in only a few cases (e.g. Talbot, Jensen & Dufour 1979). We accept outer cutoffs (e.g. van den Kruit & Searle 1981a,b, 1982). Oval disks are only piece-wise exponential. Would it be a surprise if disks also knew how to deviate above an exponential to small radii?*”

6.2 On the Origin of the Hubble Sequence

Observationally it is well established that galaxy concentration (e.g. Kauffmann et al. 2003); bulge fraction (e.g. Benson et al. 2007) and Sérsic index (e.g. this paper) increase with stellar mass. An alternative way to frame these observations is that the Hubble sequence of galaxy types is also, on average, a mass sequence. Understanding the origin of the Hubble sequence is one of the most fundamental problems in astrophysics. Here we identify four mechanisms that give plausible explanations for the observed trends. All of these mechanisms likely occur, but it remains to be determined which, if any, process dominates on any particular mass scale.

1) **Major Merger Rate:** Based on the differences in the shape of the halo mass function to that of the stel-

lar mass function, Maller (2008) showed that major galaxy mergers are more common in higher mass galaxies. For example, the largest contribution in mass comes from mergers with a mass ratio of 1:10 (e.g. Stewart et al. 2008). In a halo with mass less than about $10^{12} M_{\odot}$ a 1:10 halo mass merger ratio will result in a less than 1:10 galaxy mass merger ratio, whereas in a halo of mass greater than about $10^{12} M_{\odot}$ a 1:10 halo mass merger ratio will result in a greater than 1:10 galaxy mass ratio. Since major mergers destroy stellar disks producing spheroidal remnants (e.g. Barnes 1992; Cox et al. 2006), higher mass galaxies are expected to have higher bulge fractions.

2) **Gas Fractions:** It is observationally known that cold gas fractions are lower in higher mass galaxies (McGaugh & de Blok 1997; Kannappan 2004). For disk galaxies this is likely caused by the combined effects of the Schmidt law for star formation (in which star formation is less efficient at lower gas densities) and the effects of outflows (which result in lower density disks in lower mass galaxies). Theoretically it is known that the bulge fraction of the merger remnant increases with decreasing gas fraction of the progenitors (e.g. Springel & Hernquist 2005; Robertson et al. 2006; Hopkins et al. 2009). Thus we expect higher mass galaxies to have higher bulge fractions due to major and intermediate mass ratio mergers.

3) **Secular Evolution:** Secular (i.e. slow relative to the dynamical time of the system) processes such as bars, oval distortions and spiral structure are known to redistribute mass within disk galaxies (see Kormendy & Kennicutt 2004 for a review). A simple criterion for the onset of disk instability is the relative contribution of the disk to the total rotation velocity within the optical radius of the galaxy (e.g. Efsthathiou, Lake, & Negroponte 1982). Since the contribution of the disk to the total rotation velocity increases with stellar mass and surface brightness (e.g. Zavala et al. 2003; Pizagno et al. 2005; McGaugh 2005; Dutton et al. 2007), more massive disks are, on average, expected to be more prone to disk instabilities. Thus more massive galaxies should have larger bulge fractions and light concentrations than less massive galaxies.

4) **Feedback:** In our model the structure of the disk is determined by conservation of specific angular momentum. The mass dependence to the disk structure arises due to two effects: 1) the specific angular momentum of galaxies increases with decreasing halo mass, due to increased outflow efficiency in lower mass haloes. 2) Feedback preferentially removes low angular momentum material, which directly results in less concentrated disks. This model produces an increase in the concentration of the stellar disk with stellar mass, in agreement with observations, but without secular evolution or mergers. It is also worth pointing out that in order to produce galaxies with the observed gas fractions and standard star formation laws, feedback is required (Dutton & van den Bosch 2008).

6.3 Future Directions

There are a number of avenues for future research suggested by this paper.

6.3.1 Observations of Disk Galaxy Structure

The observational analysis of galaxy structure that we present in §4 could be greatly improved upon. The first step would be two dimensional Sérsic fits, which take account of the inclination of the disk. However, single Sérsic fits do not always provide a good match to the data, for example if there are multiple components with different axis ratios, or if there is a highly concentrated bulge/point source in the center of the galaxy (which will drive the Sérsic index artificially high). An improvement would be multi-component fits, such as bulge plus disk (e.g. Simard et al. 2002), or bulge plus disk plus bar fits (e.g. Weinzirl et al. 2008).

Rather than focusing on bulge to disk ratios, which are notoriously hard to determine (and depend implicitly on how one defines the bulge and disk), an alternative, and perhaps more useful approach would be to measure the average (and dispersion of) de projected surface brightness profiles as a function of fundamental galaxy parameters, such as stellar mass, color, and size. Not only would such a study highlight the role of fundamental galaxy parameters in determining galaxy structure, but would also provide strong observational constraints for galaxy formation models to be tested against.

Since disk galaxies often have strong color gradients, the concentration of the stellar mass may be significantly larger than that in optical light. Thus it is desirable to measure disk structural parameters in wavelengths that are more sensitive to stellar mass, and less sensitive to extinction and young stellar populations (although these are useful to study in their own right). This means near IR rest frame wavelengths.

The calculation of global stellar masses is now routine both at low and high redshift. The next step in galaxy structure studies is to apply these methods either to radial surface brightness profiles, or directly to the 2-D surface brightness maps. The feasibility and importance of these procedures have been demonstrated in spiral galaxy mass model studies (e.g. Kranz et al. 2003; Kassin et al. 2006). What is needed now is a study of the stellar mass structural properties of a statistical sample of galaxies.

An often ignored component of galaxies is the neutral and atomic gas. While the cold gas may only contribute $\simeq 10\%$ of the baryonic mass of Milky way mass galaxies, due to the atomic gas being typically more extended than the stars it is likely to contribute significantly to the angular momentum. Furthermore, the gas to stellar mass ratio increases in lower mass galaxies, and in dwarf galaxies the gas is often the dominant component. Thus to achieve a complete observational picture of galaxy structure, it is essential, especially in lower mass galaxies, to include the cold gas.

6.3.2 Improvements to Treatment of Angular Momentum in Semi Analytic Models

A necessary simplification made in our model was the assumption that the spin and AMD of the halo was, for a given halo, constant with redshift. The validity of this assumption needs to be tested with cosmological simulations.

We have shown that a subset of the AMDs found in cosmological simulations can produce close to exponential disks, once the effects of star formation and feedback are taken into account. An important question is whether the

merger histories of these haloes are consistent with the survival of a bulge-less disk. In order to address this question one needs to extend the disk evolution models discussed in this paper to full halo merger histories (e.g. Stringer & Benson 2007). However, in order to treat the build-up of angular momentum self consistently we need to know how the AMD of the halo is correlated to its merger history. For example we would like to split the AMD into that due to major mergers (which will generally destroy disks), and that due to minor mergers and smooth accretion (which will generally result in growth to the disk).

6.3.3 Initial Conditions for Secular Evolution/Merger Simulations

Numerical simulations of mergers and secular evolution are generally (but not always e.g. Debattista et al. 2004) set up assuming the disk is exponential (e.g. Springel & Hernquist 2005; Cox et al. 2006; Debattista et al. 2006; Foyle, Courteau, & Thacker 2008). The surface density profiles of our models, which are motivated by cosmological initial conditions, are in general not exponential. If these are used as initial conditions, do they result in any testable differences in galaxy structure, compared to exponential disk initial conditions. Furthermore, do secular processes, or mergers preserve or modify the stellar concentration-mass relation produced by our simple disk evolution models?

7 SUMMARY

We have used a disk galaxy evolution model to investigate the origin of the surface density profiles of disk galaxies. Our model follows the accretion, cooling and ejection of baryonic mass inside growing dark matter haloes. Contrary to most models of disk galaxy formation, we do not assume that the disk is an exponential. In our models the surface density profile of the disk is determined by the specific angular momentum distribution (AMD) of the cooled baryons and centrifugal equilibrium. For the specific angular momentum of the hot gas we use fitting functions from cosmological simulations. The galaxy mass fractions m_{gal} are determined by the efficiencies of cooling and feedback, and the stellar mass-to-light ratios are determined by the star formation history and chemical evolution of our models. We have used observations of Sérsic indices from the SDSS to constrain our feedback models and provide observational constraints on the frequency of bulge-less galaxies. We summarize our results as follows:

- We have compared two fitting formulae for the halo AMD: from Bullock et al. (2001b), and Sharma & Steinmetz (2005). In general terms these two formulae give similar results for the disk structure, but there are significant differences, especially at the tails of the distributions. It would be desirable to determine which if either of these AMD's provides a better description of the AMD's in cosmological simulations, and whether an alternative fitting function provides a better overall fit.
- Exponential and quasi-exponential stellar disks can be produced by our model through a combination of SN-driven galactic outflows (which preferentially remove low angular

momentum material), intrinsic variation in the angular momentum distribution of the halo gas, and the inefficiency of star formation at large radii.

- We use observations from the SDSS NYU-VAGC to show that the median Sérsic index of both red and blue galaxies is a strong function of stellar mass. For blue galaxies, low mass ($M_{\text{star}} \simeq 10^9 M_{\odot}$) galaxies have $n \simeq 1.3$, while high mass ($M_{\text{star}} \simeq 10^{11} M_{\odot}$) galaxies have $n \simeq 4$, with a transition mass of $M_{\text{star}} \simeq 2.5 \times 10^{10} M_{\odot}$.

- Our model with energy driven outflows correctly reproduces the observed relation between Sérsic index and stellar mass, whereas our models with momentum driven outflows and no outflows over predict the Sérsic indices in low mass galaxies. Thus the exponential density profile is not a trivial result of cosmological initial conditions.

- The observed fraction of “bulge-less” exponential galaxies is a strong function of stellar mass. For Milky-Way mass galaxies ($V_{\text{rot}} \simeq 220 \text{ km s}^{-1}$, $M_{\text{star}} \simeq 10^{11} M_{\odot}$) less than 0.1% of blue galaxies are bulge-less, whereas for M33 mass galaxies ($V_{\text{rot}} \simeq 120 \text{ km s}^{-1}$, $M_{\text{star}} \simeq 10^{10} M_{\odot}$) bulge-less and quasi-bulgeless galaxies are more common with $\simeq 45\%$ of blue galaxies having Sérsic index $n < 1.5$. These results suggest that the difficulty of hierarchical formation models to produce bulge-less Milky-Way mass galaxies (e.g. Abadi et al. 2003; Robertson et al. 2004; Okamoto et al. 2005; Governato et al. 2007) is in fact not a problem for Λ CDM. However, the problem of producing galaxies like M33 remains, and will provide a key test for hierarchical galaxy formation models, and in particular the role of feedback.

- Contrary to general assumptions, our models suggest that galaxy disks do not have a universal exponential density profile, especially at small radii.

ACKNOWLEDGEMENTS

I thank, Frank van den Bosch, Eric Bell, Stéphane Courteau, Avishai Dekel, Sandy Faber, Neil Katz, Andrea Macciò, and Julio Navarro for useful discussions. I thank the referee for providing useful suggestions for improving the manuscript. A.A.D. acknowledges support from the National Science Foundation Grants AST-0507483, AST-0808133.

Funding for the Sloan Digital Sky Survey (SDSS) has been provided by the Alfred P. Sloan Foundation, the Participating Institutions, the National Aeronautics and Space Administration, the National Science Foundation, the U.S. Department of Energy, the Japanese Monbukagakusho, and the Max Planck Society. The SDSS Web site is <http://www.sdss.org/>.

The SDSS is managed by the Astrophysical Research Consortium (ARC) for the Participating Institutions. The Participating Institutions are The University of Chicago, Fermilab, the Institute for Advanced Study, the Japan Participation Group, The Johns Hopkins University, Los Alamos National Laboratory, the Max-Planck-Institute for Astronomy (MPIA), the Max-Planck-Institute for Astrophysics (MPA), New Mexico State University, University of Pittsburgh, Princeton University, the United States Naval Observatory, and the University of Washington.

REFERENCES

- Abadi, M. G., Navarro, J. F., Steinmetz, M., & Eke, V. R. 2003, *ApJ*, 591, 499
- Abazajian, K., et al. 2004, *AJ*, 128, 502
- Baldry, I. K., Glazebrook, K., Brinkmann, J., Ivezić, Z., Lupton, R. H., Nichol, R. C., & Szalay, A. S. 2004, *ApJ*, 600, 681
- Barazza, F. D., Jogee, S., & Marinova, I. 2008, *ApJ*, 675, 1194
- Barnes, J. E. 1992, *ApJ*, 393, 484
- Bell, E. F. 2002, *ApJ*, 581, 1013
- Bell, E. F., McIntosh, D. H., Katz, N., & Weinberg, M. D. 2003, *ApJS*, 149, 289
- Bell, E. F. 2008, *ApJ*, 682, 355
- Benson, A. J., Džanović, D., Frenk, C. S., & Sharples, R. 2007, *MNRAS*, 379, 841
- Bland-Hawthorn, J., Vlahić, M., Freeman, K. C., & Draine, B. T. 2005, *ApJ*, 629, 239
- Blanton, M. R., et al. 2005, *AJ*, 129, 2562
- Blitz, L., & Rosolowsky, E. 2004, *ApJL*, 612, L29
- Blitz, L., & Rosolowsky, E. 2006, *ApJ*, 650, 933
- Blumenthal, G. R., Faber, S. M., Flores, R., & Primack, J. R. 1986, *ApJ*, 301, 27
- Bruzual, G., & Charlot, S. 2003, *MNRAS*, 344, 1000
- Bullock, J. S., Kolatt, T. S., Sigad, Y., Somerville, R. S., Kravtsov, A. V., Klypin, A. A., Primack, J. R., & Dekel, A. 2001a, *MNRAS*, 321, 559
- Bullock, J. S., Dekel, A., Kolatt, T. S., Kravtsov, A. V., Klypin, A. A., Porciani, C., & Primack, J. R. 2001b, *ApJ*, 555, 240 (B01)
- Ceverino, D., & Klypin, A. 2007, arXiv:astro-ph/0712.3285
- Chabrier, G. 2003, *PASP*, 115, 763
- Chen, D. N., Jing, Y. P., & Yoshikawa, K. 2003, *ApJ*, 597, 35
- Conroy, C., & Wechsler, R. H. 2008, arXiv:0805.3346
- Cox, T. J., Dutta, S. N., Di Matteo, T., Hernquist, L., Hopkins, P. F., Robertson, B., & Springel, V. 2006, *ApJ*, 650, 791
- Crampin, D. J., & Hoyle, F. 1964, *ApJ*, 140, 99
- Dalcanton, J. J., Spergel, D. N., & Summers, F. J. 1997, *ApJ*, 482, 659
- Davis, M., et al. 2007, *ApJL*, 660, L1
- Debattista, V. P., Carollo, C. M., Mayer, L., & Moore, B. 2004, *ApJL*, 604, L93
- Debattista, V. P., Mayer, L., Carollo, C. M., Moore, B., Wadsley, J., & Quinn, T. 2006, *ApJ*, 645, 209
- de Jong, R. S., & Lacey, C. 2000, *ApJ*, 545, 781
- Dekel, A., & Silk, J. 1986, *ApJ*, 303, 39
- de Vaucouleurs, G. 1959, *Handbuch der Physik*, 53, 311
- Domínguez-Tenreiro, R., Tissera, P. B., & Sáiz, A. 1998, *ApJL*, 508, L123
- Dunkley, J., et al. 2009, *ApJS*, 180, 306
- Dutton, A. A., van den Bosch, F. C., Dekel, A., & Courteau, S. 2007, *ApJ*, 654, 27
- Dutton, A. A., & van den Bosch, F. C. 2008, arXiv:0810.4963 (DB08)
- Efstathiou, G., Lake, G., & Negroponte, J. 1982, *MNRAS*, 199, 1069
- Eke, V., Efstathiou, G., & Wright, L. 2000, *MNRAS*, 315, L18
- Elmegreen, B. G. 1993, *ApJ*, 411, 170
- Fall, S. M., & Efstathiou, G. 1980, *MNRAS*, 193, 189
- Ferguson, A. M. N., & Clarke, C. J. 2001, *MNRAS*, 325, 781
- Firmani, C., & Avila-Reese, V. 2000, *MNRAS*, 315, 457
- Foyle, K., Courteau, S., & Thacker, R. J. 2008, *MNRAS*, 386, 1821
- Freeman, K. C. 1970, *ApJ*, 160, 811
- Gao, Y., & Solomon, P. M. 2004, *ApJ*, 606, 271
- Governato, F., et al. 2004, *ApJ*, 607, 688
- Governato, F., Willman, B., Mayer, L., Brooks, A., Stinson, G., Valenzuela, O., Wadsley, J., & Quinn, T. 2007, *MNRAS*, 374, 1479
- Gunn, J. E. 1982, *Astrophysical Cosmology Proceedings*, 233
- Hammer, F., Puech, M., Chemin, L., Flores, H., & Lehnert, M. D. 2007, *ApJ*, 662, 322
- Hoekstra, H., Hsieh, B. C., Yee, H. K. C., Lin, H., & Gladders, M. D. 2005, *ApJ*, 635, 73
- Hopkins, P. F., Cox, T. J., Younger, J. D., & Hernquist, L. 2009, *ApJ*, 691, 1168
- Kamionkowski, M., & Liddle, A. R. 2000, *Physical Review Letters*, 84, 4525
- Kannappan, S. J. 2004, *ApJL*, 611, L89
- Kassin, S. A., de Jong, R. S., & Weiner, B. J. 2006, *ApJ*, 643, 804
- Kauffmann, G., et al. 2003, *MNRAS*, 341, 54
- Kaufmann, T., Mayer, L., Wadsley, J., Stadel, J., & Moore, B. 2007, *MNRAS*, 375, 53
- Kautsch, S. J., Grebel, E. K., Barazza, F. D., & Gallagher, J. S., III 2006, *A&A*, 445, 765
- Koekemoer, A. M., et al. 2007, *ApJS*, 172, 196
- Kormendy, J., & Kennicutt, R. C., Jr. 2004, *ARA&A*, 42, 603
- Kormendy, J., & Fisher, D. B. 2005, *Revista Mexicana de Astronomía y Astrofísica Conference Series*, 23, 101
- Kranz, T., Slyz, A., & Rix, H.-W. 2003, *ApJ*, 586, 143
- MacArthur, L. A., Courteau, S., & Holtzman, J. A. 2003, *ApJ*, 582, 689
- Macciò, A. V., Dutton, A. A., van den Bosch, F. C., Moore, B., Potter, D., & Stadel, J. 2007, *MNRAS*, 378, 55
- Macciò, A. V., Dutton, A. A., & van den Bosch, F. C. 2008, *MNRAS*, 391, 1940
- Maller, A. H., Dekel, A., 2002, *MNRAS*, 363, 1155
- Maller, A. H. 2008, *ASPC*, 396, 251
- Mandelbaum, R., Seljak, U., Kauffmann, G., Hirata, C. M., & Brinkmann, J. 2006, *MNRAS*, 368, 715
- Mayer, L., Governato, F., & Kaufmann, T. 2008, *Advanced Science Letters*, 1, 7
- McGaugh, S. S., & de Blok, W. J. G. 1997, *ApJ*, 481, 689
- McGaugh, S. S. 2005, *Physical Review Letters*, 95, 171302
- Mestel, L. 1963, *MNRAS*, 126, 553
- Mo, H. J., Mao, S., & White, S. D. M. 1998, *MNRAS*, 295, 319
- Murray, N., Quataert, E., & Thompson, T. A. 2005, *ApJ*, 618, 569
- Navarro, J. F., & Benz, W. 1991, *ApJ*, 380, 320
- Navarro, J. F., & White, S. D. M. 1994, *MNRAS*, 267, 401
- Navarro, J. F., Frenk, C. S., & White, S. D. M. 1997, *ApJ*, 490, 493
- Navarro, J. F., & Steinmetz, M. 2000, *ApJ*, 538, 477
- Noeske, K. G., et al. 2007, *ApJL*, 660, L43
- Okamoto, T., Eke, V. R., Frenk, C. S., & Jenkins, A. 2005, *MNRAS*, 363, 1299
- Olivier, S. S., Primack, J. R., & Blumenthal, G. R. 1991, *MNRAS*, 252, 102
- Pizagno, J., et al. 2005, *ApJ*, 633, 844
- Pohlen, M., & Trujillo, I. 2006, *A&A*, 454, 759
- Rix, H.-W., et al. 2004, *ApJS*, 152, 163
- Robertson, B., Yoshida, N., Springel, V., & Hernquist, L. 2004, *ApJ*, 606, 32
- Robertson, B., Bullock, J. S., Cox, T. J., Di Matteo, T., Hernquist, L., Springel, V., & Yoshida, N. 2006, *ApJ*, 645, 986
- Roškar, R., Debattista, V. P., Stinson, G. S., Quinn, T. R., Kaufmann, T., & Wadsley, J. 2008, *ApJL*, 675, L65
- Schmidt, M. 1959, *ApJ*, 129, 243
- Scoville, N., et al. 2007, *ApJS*, 172, 1
- Sharma, S., & Steinmetz, M. 2005, *ApJ*, 628, 21 (SS05)
- Simard, L., et al. 2002, *ApJS*, 142, 1
- Sommer-Larsen, J., Gelato, S., & Vedel, H. 1999, *ApJ*, 519, 501
- Sommer-Larsen, J., & Dolgov, A. 2001, *ApJ*, 551, 608
- Springel, V., & Hernquist, L. 2005, *ApJL*, 622, L9
- Stewart, K. R., Bullock, J. S., Wechsler, R. H., Maller, A. H., & Zentner, A. R. 2008, *ApJ*, 683, 597

- Stringer, M. J., & Benson, A. J. 2007, *MNRAS*, 382, 641
- Sutherland, R. S., & Dopita, M. A. 1993, *ApJS*, 88, 253
- Talbot, R. J., Jr., Jensen, E. B., & Dufour, R. J. 1979, *ApJ*, 229, 91
- Tully, R. B., & Fisher, J. R. 1977, *A&A*, 54, 661
- van den Bosch, F. C. 2001, *MNRAS*, 327, 1334
- van den Bosch, F. C. 2002a, *MNRAS*, 332, 456
- van den Bosch, F. C., Abel, T., Croft, R. A. C., Hernquist, L., & White, S. D. M. 2002, *ApJ*, 576, 21
- van der Kruit, P. C., & Searle, L. 1981, *A&A*, 95, 105
- van der Kruit, P. C., & Searle, L. 1981, *A&A*, 95, 116
- van der Kruit, P. C., & Searle, L. 1982, *A&A*, 110, 61
- Wechsler, R. H., Bullock, J. S., Primack, J. R., Kravtsov, A. V., & Dekel, A. 2002, *ApJ*, 568, 52
- Weil, M. L., Eke, V. R., & Efstathiou, G. 1998, *MNRAS*, 300, 773
- Weinzirl, T., Jogee, S., Khochfar, S., Burkert, A., & Kormendy, J. 2008, *arXiv:astro-ph/0807.0040*
- Widrow, L. M., Pym, B., & Dubinski, J. 2008, *ApJ*, 679, 1239
- White, S. D. M., & Rees, M. J. 1978, *MNRAS*, 183, 341
- Wong, T., & Blitz, L. 2002, *ApJ*, 569, 157
- Wu, J., Evans, N. J., II, Gao, Y., Solomon, P. M., Shirley, Y. L., & Vanden Bout, P. A. 2005, *ApJL*, 635, L173
- Yang, X., Mo, H. J., van den Bosch, F. C., Pasquali, A., Li, C., & Barden, M. 2007, *ApJ*, 671, 153
- Younger, J. D., Cox, T. J., Seth, A. C., & Hernquist, L. 2007, *ApJ*, 670, 269
- Zavala, J., Avila-Reese, V., Hernández-Toledo, H., & Firmani, C. 2003, *A&A*, 412, 633